AD_____

Award Number DAMD17-94-J-4032

TITLE: Breast Cancer Cell Metabolism Studied by MRS

PRINCIPAL INVESTIGATOR: Raymond L. Woosley, M.D.

CONTRACTING ORGANIZATION: Georgetown University
Washington, DC 20057

REPORT DATE: September 1999

TYPE OF REPORT: Final

PREPARED FOR: U.S. Army Medical Research and Materiel Command
Fort Detrick, Maryland 21702-5012

DISTRIBUTION STATEMENT: Approved for Public Release;
Distribution Unlimited

The views, opinions and/or findings contained in this report are those of the author(s) and should not be construed as an official Department of the Army position, policy or decision unless so designated by other documentation.

REPORT DOCUMENTATION PAGE

Form Approved
OMB No. 0704-0188

1. AGENCY USE ONLY *(Leave blank)*	2. REPORT DATE	3. REPORT TYPE AND DATES COVERED
	September 1999	Final (1 Jul 94 - 31 Aug 99)

4. TITLE AND SUBTITLE
Breast Cancer Cell Metabolism Studied by MRS

5. FUNDING NUMBERS
DAMD17-94-J-4032

6. AUTHOR(S)
Raymond L. Woosley, M.D.

7. PERFORMING ORGANIZATION NAME(S) AND ADDRESS(ES)
Georgetown University
Washington, DC 20057

8. PERFORMING ORGANIZATION REPORT NUMBER

9. SPONSORING / MONITORING AGENCY NAME(S) AND ADDRESS(ES)
U.S. Army Medical Research and Materiel Command
Fort Detrick, Maryland 21702-5012

10. SPONSORING / MONITORING AGENCY REPORT NUMBER

11. SUPPLEMENTARY NOTES

12a. DISTRIBUTION / AVAILABILITY STATEMENT
Approved for Public Release; Distribution Unlimited

12b. DISTRIBUTION CODE

13. ABSTRACT *(Maximum 200 words)*

Many breast tumors progress from estrogen-dependent growth to a more malignant phenotype, characterized by estrogen-independence, anti-estrogen resistance, and high metastatic potential. We have investigated this transition utilizing magnetic resonance (MR) techniques on a series of cell lines selected to reflect the characteristics of this progression. Using phosphorus-31 MR spectroscopy we monitored intracellular phosphate-containing molecules, and found significant differences between the ER^+ and ER^- cell lines only for the diphosphodiester components that we assigned to UDPG's (where G is glucose and galactose). We added a series of anti-cancer drugs, and found a significant increase in the glycerylphosphocholine (GPC) signal with the anti-microtubule drugs, and showed that this was not due to cell cycle effects by carrying out cell synchronization experiments. We also developed and applied proton diffusion weighted (DW) MRS to the cell lines to observe intra-cellular metabolites. While many peaks were unchanged between the cell lines, some peak ratios showed differences between two groups of cell lines. We were able to observe the intra-cellular lactate resonance, and to monitor its increase upon the addition of the anti-cancer agent lonidamine. These results add to our understanding of these cell lines and may be of value in future clinical MR applications to breast cancer treatment.

14. SUBJECT TERMS
Breast Cancer

15. NUMBER OF PAGES
40

16. PRICE CODE

17. SECURITY CLASSIFICATION OF REPORT	18. SECURITY CLASSIFICATION OF THIS PAGE	19. SECURITY CLASSIFICATION OF ABSTRACT	20. LIMITATION OF ABSTRACT
Unclassified	Unclassified	Unclassified	Unlimited

FOREWORD

Opinions, interpretations, conclusions and recommendations are those of the author and are not necessarily endorsed by the U.S. Army.

____ Where copyrighted material is quoted, permission has been obtained to use such material.

____ Where material from documents designated for limited distribution is quoted, permission has been obtained to use the material.

____ Citations of commercial organizations and trade names in this report do not constitute an official Department of Army endorsement or approval of the products or services of these organizations.

____ In conducting research using animals, the investigator(s) adhered to the "Guide for the Care and Use of Laboratory Animals," prepared by the Committee on Care and use of Laboratory Animals of the Institute of Laboratory Resources, national Research Council (NIH Publication No. 86-23, Revised 1985).

✓ For the protection of human subjects, the investigator(s) adhered to policies of applicable Federal Law 45 CFR 46.

____ In conducting research utilizing recombinant DNA technology, the investigator(s) adhered to current guidelines promulgated by the National Institutes of Health.

____ In the conduct of research utilizing recombinant DNA, the investigator(s) adhered to the NIH Guidelines for Research Involving Recombinant DNA Molecules.

____ In the conduct of research involving hazardous organisms, the investigator(s) adhered to the CDC-NIH Guide for Biosafety in Microbiological and Biomedical Laboratories.

Jack Stoh 9/3/99

PI - Signature / Date

TABLE OF CONTENTS

1. INTRODUCTION

A. Scientific Background

In order to elucidate the processes involved in the development and possible treatment of breast cancer, we have investigated the metabolism of intact breast cancer cells using magnetic resonance spectroscopy (MRS) methods.

Magnetic Resonance Spectroscopy Methods

It is well known that magnetic resonance techniques have become important in clinical imaging, but perhaps less well known is the fact that MRS can be used as a research tool to study the metabolism of packed, perfused, intact cells (Daly and Cohen, 1989). Such studies have provided information on biochemical processes *in vitro*, and can be used for the identification of MR signals and the consequent understanding of metabolic processes *in vivo*. ^{31}P MRS studies have provided information on normal cellular energetic status, substrate utilization and metabolic pathways, phospholipid pathways, intra-cellular pH changes and membrane permeability. Using this method, significant metabolic differences between cell lines have been delineated, and effects on metabolism following manipulation with nutrients, hormones, drugs, growth factors, and hyperthermia have been monitored (for a review see Cohen et al, 1995).

Although proton (^{1}H) MRS is intrinsically 14 times more sensitive than ^{31}P MRS, very little research has been done using ^{1}H MRS on cell metabolism *in vitro* (Cohen et al, 1995), even though ^{1}H MRS studies have been reported *in vivo* (Kvistad et al, 1999). There are three main reasons for this apparent anomaly: (a) the overlap of the many signals from hundreds of metabolites, (b) the presence of the huge water signal in biological systems, and (c) the overlap of signals from intra-cellular and extra-cellular substances, including buffers, metabolites, etc. Reasons (b) and (c) can be overcome by the use of a diffusion-weighted (DW) MRS technique, whereby the application of two magnetic field gradient pulses allows for the selection of a time window for the observation of slowly moving molecules only. A technique for diffusion measurements first implemented by Stejskal and Tanner in 1965 was the pulsed gradient spin echo (PGSE) method. DWMRS eliminates the signals of most of the water and extra-cellular molecules that are moving rapidly, and allows one to observe the proton signals from intra-cellular molecules only (Van Zijl et al, 1991).

However, there is still extensive overlap of metabolite signals at 400 MHz, causing difficulties in resolution and assignment of signals. As was done in the field of ^{1}H MRS studies of proteins to overcome this resolution problem, the best way is to increase the magnetic field strength. Thus, we extended our studies of cancer cell metabolism with DWMRS at 600 MHz, using the instrument at Bar-Ilan University. To our knowledge no proton MRS studies of cellular metabolism have previously been reported at this high field strength.

Another advantage of ^{1}H MRS is that, because of its higher sensitivity, fewer cells will be needed to obtain spectra. The intrinsic sensitivity should give rise to approximately an order of magnitude improvement in the speed to obtain spectra (this is without considering the longer relaxation times for ^{31}P nor the extra times required for the diffusion weighting pulses in ^{1}H MRS). Since fewer cells are needed, the cost of the experiments will go down and many more experiments should be possible with fewer cells in less time. Another difference related to the difference in sensitivity is that ^{31}P MRS probes use 10 mm tubes and proton MRS probes generally use 5 mm tubes. But, previous attempts (unpublished) to build a 5 mm perfusion system, have encountered difficulties, largely due to the problem of obtaining water resistant seals in such small tubes. Also, the capillary tubing used to deliver and remove the perfusate takes up a considerable portion of the internal volume of the 5 mm tube, thus displacing many cells. Fortunately, the 600 MHz instrument at Bar-Ilan University has an 8 mm ^{1}H probe that is equipped with a magnetic gradient system. This is a good compromise for ^{1}H MRS studies between the unnecessarily large size of 10 mm tubes and the too small size of 5 mm for construction of a workable perfusion system.

Cell Perfusion Methods

Perfused intact cells represent possibly the best approach to the non-invasive study of metabolism *in vitro*. In contrast to the *in vivo* situation, the cells are homogeneous, particularly when grown in culture conditions. A variety of methods for restraining cells for MRS studies of metabolism are currently available. The techniques chosen by us use gels to embed the cells. The advantages of these method are: (a) they are simple, inexpensive

and easy to use; (b) a large number of cells can be maintained in good metabolic status for prolonged periods (up to 72 hr); (c) the matrix itself occupies a relatively small volume (as opposed to the use of beads); (d) effects on metabolism due to the addition of metabolite precursors (nutrients) or drugs, or physical changes (such as temperature) can be detected immediately; and (e) both anchorage-dependent and -independent (cancer) cells can be studied. Detailed studies of cell growth and viability (using trypan blue exclusion and cell counting), cell microscopy, and measurement of diffusion constants of metabolites (ATP, glucose) were previously carried out using cells embedded in agarose gel threads (Foxall and Cohen, 1983; Foxall et al, 1984; Knop et al, 1984; Lyon et al, 1986; Kaplan et al, 1990). Also, alginate capsules have been described as a very convenient approach to embed cells in gel (Lim and Moss, 1981), and this method has been applied to several cell types (Shankar-Narayan et al., 1990; Kaplan and Cohen, 1991).

One of the disadvantages of perfusion studies with agarose threads is the lack of proliferative activity inside the threads. Agarose is a carbohydrate gel, and in the agarose method cells are "trapped" in the threads and can be removed by gentle pipetting. Matrigel is a natural basement membrane and is a protein gel for which breast cancer cells have receptors, mainly for collagen IV. It is an extremely open gel that is used extensively for studies of cancer cells (Kleinman et al, 1986). The gel thread technique was therefore improved by the use of a Matrigel, in which anchorage-dependent cells can multiply while being perfused (Daly et al, 1988). Dispase was used to dissolve Matrigel in order to measure cell densities (Daly et al, 1988). It should also be emphasized that a comparison of the same cell line in Matrigel cell threads and in tumor xenografts in nude mice gave almost identical spectra (Daly et al, 1988). We have chosen the Matrigel threads as the most effective system in which the effects of cell growth and hormone dependence can be monitored.

Hormone Dependence of Breast Cancer Cells and Drug Effects

In order to understand the role of estrogen receptor (ER) status in breast cancer cells Clarke et al. (1989, 1990), have selected cell lines (see **Table 1**). The cell lines to be studied in this work are all variants that have been selected and extensively characterized, and exhibit specific phenotypic changes that reflect critical characteristics of the progression in therapy from hormone sensitive to insensitive phenotype. The ability to detect specific metabolic changes associated with phenotypic changes is substantially increased, since several of these cell lines were derived from the same parental cell line (MCF-7).

In breast cancer cells and other malignant cell lines, some of the cellular effects of "anti-microtubule" drugs are modulated by the action of steroids, estrogens and anti-estrogens, and vice versa. For example, Colchicine was reported to inhibit translocation of estradiol receptors and the synthesis of progesterone receptors in MCF-7 cells (Parikh et al, 1987); and to sensitize the activation of large conductance chloride channels in fibroblasts upon exposure to extra-cellular anti-estrogens (Hardy and Valverde, 1994). Tamoxifen increases the cytotoxicity of Vinblastine in MCF-7 variants which express gp170 (Leonessa et al., 1994) and reversed Vinblastine resistance in the mdr1 transfected lung cancer cell line, S1/1.1 (Kirk et al, 1993). The anti-estrogen Toremifene, 'resensitizes' MDA-MB-231-A1, an estrogen receptor negative breast cancer cell line, to Vinblastine (Koester et al., 1994). The estrogen metabolite, 17 beta-estradiol glucuronide modulate resistance to Taxol and Vinblastine in the Dx5 MDR sarcoma cell line (Gosland et al., 1993). It was recently reported that a metabolite of estradiol, 2-methoxyestradiol, inhibits tubulin polymerization by binding to the Colchicine binding site on tubulin dimer (Cushman et al., 1995).

Among the anti-cancer drugs that will be examined are Taxol, Vincristine and Adriamycin. Taxol is an anticancer drug that has been approved for the treatment of refractory ovarian cancer, and is showing promising activity in malignant melanoma, breast cancer, and lung cancer (see McGuire and Rowinsky, 1995). Taxol has demonstrated substantial single agent activity against both minimally pretreated and resistant metastatic breast cancer (Wong and Henderson, 1994). Taxol and Vincristine are anti-mitotic drugs that interfere with the assembly process of microtubules. Microtubule functions in cells are highly complex. Aside from serving as passive skeletal supports for the organization of the cytoplasm, their remarkable polymerization dynamics is critical to many of their functions. Drugs such as Taxol and Vincristine interact with microtubule ends and surfaces and modulate the polymerization dynamics. Although all of these drugs bind to tubulin, they exert distinct effects on the protein organization in the cell. In the presence of Taxol highly organized bundles of microtubules are formed, while Vinblastine induces tubulin self-association to paracrystal formations (for a review see Wilson and Jordan, 1994). These drugs inhibit cell proliferation and replication, induce multi-drug resistance, and have a variety of cellular effects, apparently unrelated to their action on tubulin. These and other drugs have been included in this study.

B. Specific Aims

- To characterize the growth of several related human breast cancer cell lines in the natural (protein) basement membrane gel Matrigel by ^{31}P MRS spectroscopy, and to compare the role of estrogen receptor (ER) status in ER positive and ER negative cell lines on their ^{31}P MR spectra.

- To observe the effects of hormones, such as estrogen and tamoxifen, on the growth and metabolism of these cell lines, and to investigate the effects of drugs, notably Taxol, on these cell lines with different ER status and hormone dependence.

- To explore the application of ^{1}H MRS to study cancer cell metabolism with water signal suppression and observation of only intra-cellular signals, and to investigate the resolved proton signals in breast cancer cell spectra, and in response to an appropriate drug.

2. BODY OF REPORT

A. Experimental Methods

(i) Materials: Matrigel was prepared with modifications according to Kleinman et al., 1986, and Kibbey, 1994. The following materials were purchased: MatriSperse (Collaborative Biomedical Products, MA) DMEM, Fetal Calf Serum (Biological Industries, Israel), RNase A, Propidium Iodide, Vincristine, Colchicine, Nocodazole, Adriamycin, and Methotrexate (Sigma, St Louis, MO), Tissue solubilizer BTS-450 (Beckman). Taxol was a gift by Bristol Myers Squibb. Usually the drugs were dissolved in DMSO for cell work. Final DMSO concentration was 0.1% v/v. One batch of Fetal Calf Serum was used for the entire study. Charcoal stripped Fetal Calf Serum was prepared as described previously (Clarke et al., 1989).

(ii) Cell culture: Cell lines were a generous gift of Dr. Robert Clarke (Georgetown University, Washington DC, USA) (**Table 1**). MDA-MB231, MDA-MB435 and MCF7 cells were routinely maintained in DMEM and supplemented with 5% fetal calf serum. LCC2 and MIII cells were maintained in DMEM without phenol red (which has an estrogenic-like activity; Levenson and Jordan, 1997) and supplemented with 5% charcoal-stripped calf serum. All cell cultures were maintained at 37°C in a humidified 5% CO_2/ 95% air atmosphere incubator. For each MRS experiment 10 petri dishes (10 cm diameter) were plated. The amounts of cells plated for experiment were: (MDA-MB231 - 350,000 cells/dish; MDA-MB435 - 1,000,000 cells/dish; LCC2 and MIII 4,500,000 cells/dish, MCF7 1,500,000 cells/dish. After 3 days, the medium was replaced and cells were harvested for the experiment after an additional 2 days.

Table 1: Characteristics of cell lines.

Cell Line	ER	[1]Estrogen Dependence	[2]Estrogen Responsive	TAM Responsive	ICI 182,780 Responsive	Metastases
MCF7	+ ve	dependent	responsive	sensitive	sensitive	no
MIII	+ ve	independent	responsive	sensitive	sensitive	yes
LCC2	+ ve	independent	responsive	resistant	sensitive	ND[3]
LY2	+ ve	responsive	resistant	resistant	resistant	NT[4]
MDA-MB231	- ve	independent	unresponsive	resistant	resistant	yes
MDA-MB435	- ve	independent	unresponsive	resistant	resistant	yes

1 = requirement for E2 to form tumors in nude mice; 2 = respond to E2 by inducing specific genes/mitogenesis; 3 = no data; 4 = non-tumorigenic.

(iii) Cell Perfusion Methods: The use of agarose threads is based on the properties of low-temperature gelling agarose, that allows the mixing of cells with liquid agarose at 37°C, and solidification of the mixture at a lower temperature. Cell pellet (1-1.2 ml containing ca 2 x 10^8 cells) is mixed with an equal volume of liquid agarose (1.8%) in phosphate-buffered saline, and immersed in a bath at 37°C for 5-7 min. The mixture is extruded under low pressure through cooled capillary tubing (0.5 mm id) into an MRS tube containing growth medium (**Fig. 1 upper**)(for a complete description see Cohen et al, 1989). Using 0.5 mm threads ensures that the threads maintain their mechanical strength and the cells are not metabolically compromised, and are viable and in stable energetic status for more than 24 h. Moreover, it was shown that albumin can readily diffuse into the threads (Kaplan et al, 1990). The gel threads, which fill the tube, are concentrated at the bottom of the tube by insertion of a plastic insert with the perfusion fittings.

Alginate capsules were prepared by dripping a mixture of the cells (from a pellet of 0.5-0.6 ml) in an equal volume of sodium alginate solution from a capillary into a calcium chloride solution. This causes immediate gelling, and the micro-capsules are harvested by decantation. This method was favored for the ^{1}H MRS studies due to the small volume inside the MR tube.

Preparation of Matrigel threads: Cells were harvested, centrifuged, and the pellet, kept on ice, was mixed with liquid Matrigel at 4°C. The ratio between the number of cells and Matrigel volume was determined for each type of experiment. A portion of the mixture was pulled into plastic tubing that was attached to a syringe and left to solidify at room temperature for 15-60 sec. The thread was extruded into a petri dish or into a flask containing medium. Each thread was 60 cm long and 0.5 mm in diameter. Sterility was maintained during the whole procedure. To test for viability and proliferation in the perfusion system, 12 threads were prepared from 19,000,000 cells/ml Matrigel of MCF-7 cells. The threads were transferred to a sterilized MRS tube, and the tube connected to the sterilized perfusion system. ^{31}P MR spectra were taken at different time points during 72 hours.

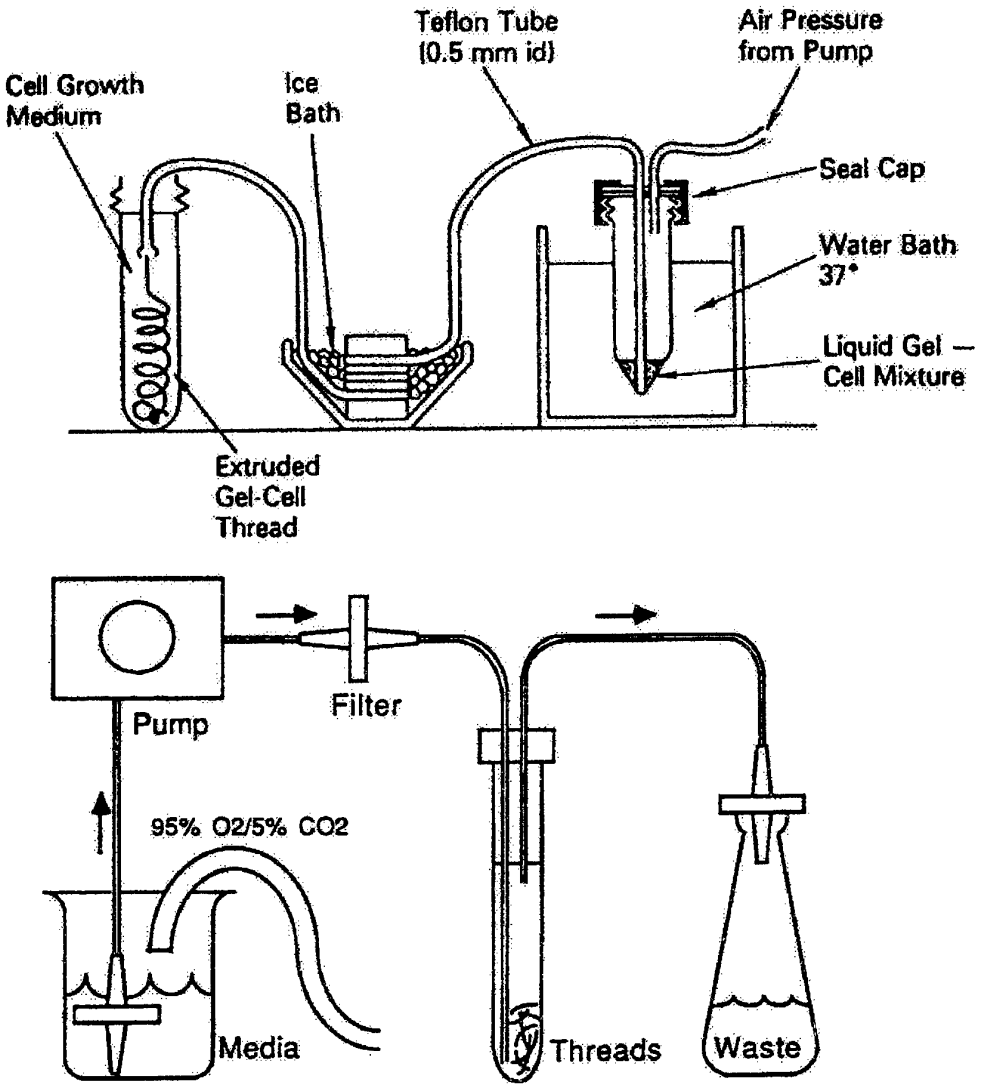

Figure 1. Upper. Extrusion method for preparing agarose threads containing cells. **Lower. Perfusion system** used in the MRS experiment

The perfusion system used (**Fig. 1 lower**) was described previously (Daly 88). The inflow tube is 0.5 mm id, and is placed near the bottom of the tube. The outflow is directed into openings in the insert, and then into an outflow tube. Perfusion rates (0.3-2 ml/min) were maintained using a peristaltic pump. Prior to the experiment, the system was sterilized by 70% ethanol, then washed with sterile water and medium in a sterile hood. The cells were perfused continuously with appropriate fresh media at 37°C, and sterile conditions were maintained by continuous filtration on line using 0.25 μm filters. The perfusion solution is the buffered growth medium that is most appropriate for the cells studied. The medium was bubbled gently with a mixture of 5% CO_2/95% O_2 to ensure sufficient oxygenation and to maintain a physiological pH. The medium container and the MRS probe were maintained at 37°C.

(iv) Phosphorus-31 MRS Methods: ^{31}P MR spectra of perfused cells embedded in Matrigel, were recorded on a AMX-400 WB Bruker instrument with a 10 mm probe, operating at 162 MHz (2s delay time and a 60° flip angle). 1000 scans were accumulated for each spectrum totaling 1 hour, and processed using 10 Hz line broadening. Peak areas were calculated as the ratio to the β-ATP signal. ^{31}P MR spectra of extracts were recorded on a vxr300s Varian spectrometer operating at 121 MHz (2 s delay time and a 60° flip angle). 1500 scans were accumulated for each spectrum totaling 1.5 hr and processed using 3 Hz line broadening.

(v) Proton MRS Methods

^{1}H MR spectra were recorded on a Bruker DMX spectrometer operating at 600 MHz with a txi8mm probe with one gradient in the z direction of 50 G/cm. Cells were embedded in sodium alginate capsules, perfused with the growth medium at 1 ml/min and 37°C, and ^{1}H MR spectra were recorded periodically. The pulse sequence is a stimulated echo sequence, which consists of three 90° rf pulses with the addition of two diffusion weighting gradients (Stejskel and Tanner, 1965). Additional intra-cellular water suppression was performed with chemical-shift-selective (CHESS) rf pulses (Moran, 1982) followed by gradient dephasing (for more details see below).

Theory of DWMRS: (non-experts may want to skip this section) Any magnetic field gradient imposed in an NMR experiment causes the spins to acquire spatially dependent phase shifts via their respective resonance (Larmor) frequencies. In conventional spin-echo MRS experiments an echo is created by a 180° rf pulse, which restores the amplitude of the signal by refocusing all phase shifts associated with inhomogeneity of the field. In the PGSE method a magnetic field inhomogeneity is deliberately generated in order to measure molecular self-diffusion. Two narrow gradient pulses of equal amplitude and duration are applied to the system, and their separation in time, Δ provides a time window during which diffusion can be detected. The 180° rf pulse is applied at time $\Delta/2$ after the first gradient pulse, so that in the absence of diffusion the spin-echo would restore the original signal. Because of the stochastic nature of Brownian motion, molecular diffusion in the presence of a spatially dependent magnetic field leads to an incoherent succession of phase shifts that will not be refocused in a spin-echo. The resultant echo attenuation may give an indication of the molecular self-diffusion coefficient, D. Because the relaxation time (the time it takes the magnetization vector to return to the steady state) is usually short in biological samples, it is desirable to minimize signal loss by replacing the PGSE sequence with one in which the 180° rf pulse is replaced by two 90° rf pulses. In order to further suppress the water signal we add a chemical shift selective saturation (CHESS) sequence, which consists of a selective 90° rf pulse followed by gradient dephasing, prior to the first and third rf pulses (Moonen and Van Zijl, 1990). A schematic representation of the pulsed gradient stimulated echo sequence is shown in **Figure 2**.

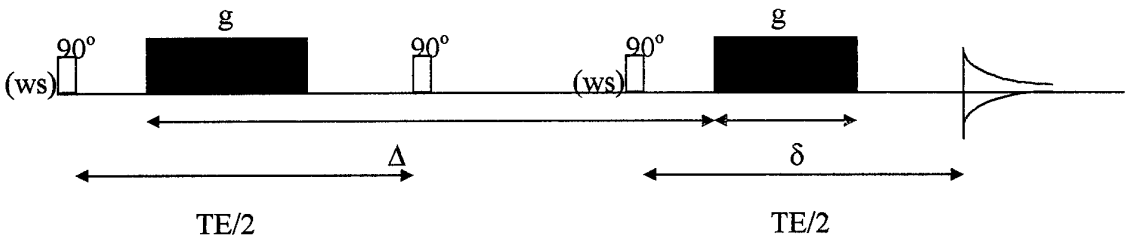

Figure 2. Pulsed gradient stimulated echo sequence used for diffusion-weighted spectroscopy. (ws) indicates optional CHESS water suppression. The white blocks represent rf pulses, and the black blocks represent gradients with intensity g.

In the case of the pulsed gradient method the intensity of the water signal is given by:

$$I/I_0 = \exp[-\gamma^2\delta^2 g^2(\Delta-\delta/3)D] = \exp[-\mathbf{b}D] \qquad (1)$$

Where, I and I_0 are signal intensities in the presence and absence of diffusion sensitizing gradients, γ is the gyromagnetic ratio of the nuclei, g and δ are gradient strength and duration, respectively, $(\Delta - \delta/3)$ is the effective diffusion time, and **b** is the diffusion weighting factor, which is expressed in units of s/cm^2. By varying g, δ and\or Δ, a diffusion curve can be obtained (Van Zijl et al., 1991), and from the slope of the logarithmic dependence of the echo amplitude on **b** one can calculate the apparent diffusion coefficient (D) (see **Fig. 20**). In biological systems there are usually several spin populations with different ADCs, so that the signal attenuation is not mono-exponential. In the simplest case, of a two-compartment system with very slow exchange between these two compartments, the attenuation of the water signal should be a bi-exponential function of **b**, with the smaller value for D originating from the intra-cellular molecules and the higher value of D arising from the sum of the intra- plus extra-cellular molecules.

(vi) Cell cycle characterization by FACS: After trypsinization or release from Matrigel threads, cells were washed twice with PBS. 2-2.5 million cells were centrifuged, resuspended in PBS and fixed by ice cold ethanol. The cells were kept on ice for 1 hour, then stored at –20°C until the analysis. Prior to analysis, cells were centrifuged and resuspended in PBS. Cells were treated with RNase A (10 mg/ml) for 30 min. at 37°C, then incubated with Propidium Iodide (0.5 mg/ml) and 1% Triton for 30 min at room temperature. Measurements were performed on Becton Dickinson FACScan.

(vii) Determination of growth curves: Different cell lines were embedded in Matrigel threads Each thread was extruded into petri dish containing 10 ml of medium. The concentration of cells in Matrigel thread, depends on the proliferation profile of each cell line. In all experiments, cells have not reached confluency: MBA-MD231, MBA-MD435 - 500,000 cells/ml; and LCC2, MIII, MCF7 - 1,000,000 cells/ml. 4 ml of Matrigel was used for each experiment. The dishes were placed in incubator. At each time point 2 threads were dissolved. Each thread was transferred to a plastic tube, washed with ice cold PBS and dissolved by 1 ml MatriSperse (1 hour on ice). The number of cells was determined by hemocytometer slide.

(viii) Drug treatments: To insure adequate drug penetration, cells were preloaded with the relevant drug by incubating the harvested cells in solution containing the desired drug concentration, for 1 hour. The cells were stirred every 10 min to prevent attachment. Thereafter, the cells were centrifuged, cooled on ice and mixed with liquid Matrigel at 4°C (1 part cells:3 parts Matrigel).

Drug time-course experiments: After preloading with drug (or DMSO for the control) and mixing with Matrigel as described above, threads were prepared as described before and placed into a flask containing 50 ml medium and the desired concentration of drug. Threads were transferred to a sterilized perfusion system. ^{31}P MR spectra were taken at several time points through 48 hours experiment. As a control, analogous procedure was performed using solution of 0.1% DMSO in medium instead of medium with drug (all drugs were dissolved in DMSO. In all experiments, DMSO concentration in the experimental solution never exceeded 0.1%, which has no effect on cell well beings). Samples of threads were taken at the beginning of the experiment, after 24 hours and at the end-point of MRS measurement after 48 hr, cells were released from the threads by Matrisperse, fixed and analyzed for cell cycle distribution by FACS, as described above.

Drug end-point experiments: After preloading with drug (or DMSO for the control) and mixing with Matrigel as described above, threads were extruded into flasks containing 120 ml medium with the experimental concentration of drug (or 0.1 % DMSO). The flasks were kept in the incubator for 48 hr (or for 24 hr when treated with Nocodazole) and after that the threads were transferred into a MRS tube, the tube was attached to the perfusion system and spectra were taken for drug treated and for control samples. A sample of a thread was taken after 24 hr and at the point of the MRS measurement, cells were released from the threads by Matrisperse, fixed and analyzed for cell cycle distribution by FACS as described above.

(ix) Synchronization in G2/M: 300,000 MDA-MB231 cells were plated per dish. After 4 days of culture, medium was changed to medium containing $3.3x10^{-7}$M Nocodazole for 12 hours. The cells were washed for 3 hours with fresh medium and harvested. At that point, a sample of the cells was taken, fixed and analyzed by FACS to ensure that cells were arrested in G2/M phase. The results were that 80-90% of the cells were in G2/M. The synchronized cells were used immediately or kept for further experiments

(x) Drug uptake by Matrigel: The uptake of Taxol into Matrigel threads was investigated. Four experimental groups were prepared. The threads (20 cm long) with 3,500,000 cells/thread or without cells, were immersed in medium containing $5x10^{-6}$ M ^{3}H-Taxol. A third set of threads was prepared with preloading. The harvested cells were incubated in a solution containing $5x10^{-6}$ M ^{3}H-Taxol for 1 hour, then centrifuged, and the pellet was mixed with liquid Matrigel (3,500,000 cells/ml). From this point the threads were prepared as without preloading. In the fourth set, cells growing as monolayers on plastic dishes were incubated with $5x10^{-6}$ M of ^{3}H-Taxol. At the designated time points, threads or monolayers were washed with ice cold PBS and dissolved overnight, in 400 µl of Tissue Solubilizer (GTS-450), after which 12 ml of scintillation solution (2 parts Toluene: 1 part Lumax) were added and radioactivity counted in a β-counter. In a parallel experiment, the number of cells per thread or in monolayers were determined by solubilizing threads in MatriSperse, or by harvesting by trypsinisation for monolayers, and counting the number of cells. The amount of radioactivity per cell for cells embedded in threads was calculated by subtracting the radioactivity of bare thread from the radioactivity of thread loaded with cells and dividing by the number of cells per thread. The amount of radioactivity per cell for cells grown in monolayer was calculated by dividing the radioactivity by the number of cells.

(xi) Extracts: For extracts of cells grown as monolayer: 10 petri dishes of 90% confluent cells were harvested, washed by ice cold saline and pelleted. 3 ml of ice cold PCA (0.5M) was added and mixed, the suspension was sonicated for 5 min at 4°C. The extract was neutralized with 5 M KOH and then centrifuged at 10,000 rpm for 10 min to precipitate the potassium perchlorate. The supernatant was treated with Chelex 100 (50 mg/ml). After filtration (to remove Chelex beads) the pH was brought to 8, supernatant was lyophilized and stored at – 20°C. For MRS analysis the lyophilized sample was dissolved in 250 µl D_2O and 250 µl solution containing 20 mM EDTA and $3x10^{-3}$ M of trimethyl phosphonoacetate as a standard. For extracts of cells embedded in Matrigel threads: threads from drug treatment experiment (12 threads, 60 cm each) were washed twice with ice cold saline by centrifugation, mixed with 3-5 ml of ice cold PCA, that caused the dissolution of the threads. From this point proceeded as for monolayer. Phospholipid extracts were performed as described previously (Tyagi et al., 1996; Meneses and Glonek, 1988).

B. Results

(i) Cell Cycle Measurements

The cell-cycle characteristics of each cell line in the non-confluent state were checked by FACS. LCC2 and MIII have somewhat reduced S levels, while MB-MDA-435 cells show elevated levels of S phase (**Fig. 3**). To check if growing in Matrigel thread changes the cell cycle distribution, MDA-MB231cells were grown in Matrigel threads, the cells were liberated by dissolving the thread with Matrisperse solution, and the cell cycle distribution was assigned by FACS. The result was not significantly different compared to cells grown on plastic. Cells grown nearly to confluence, such as those used for MRS experiments were shown to be 65-75% synchronized in G1.

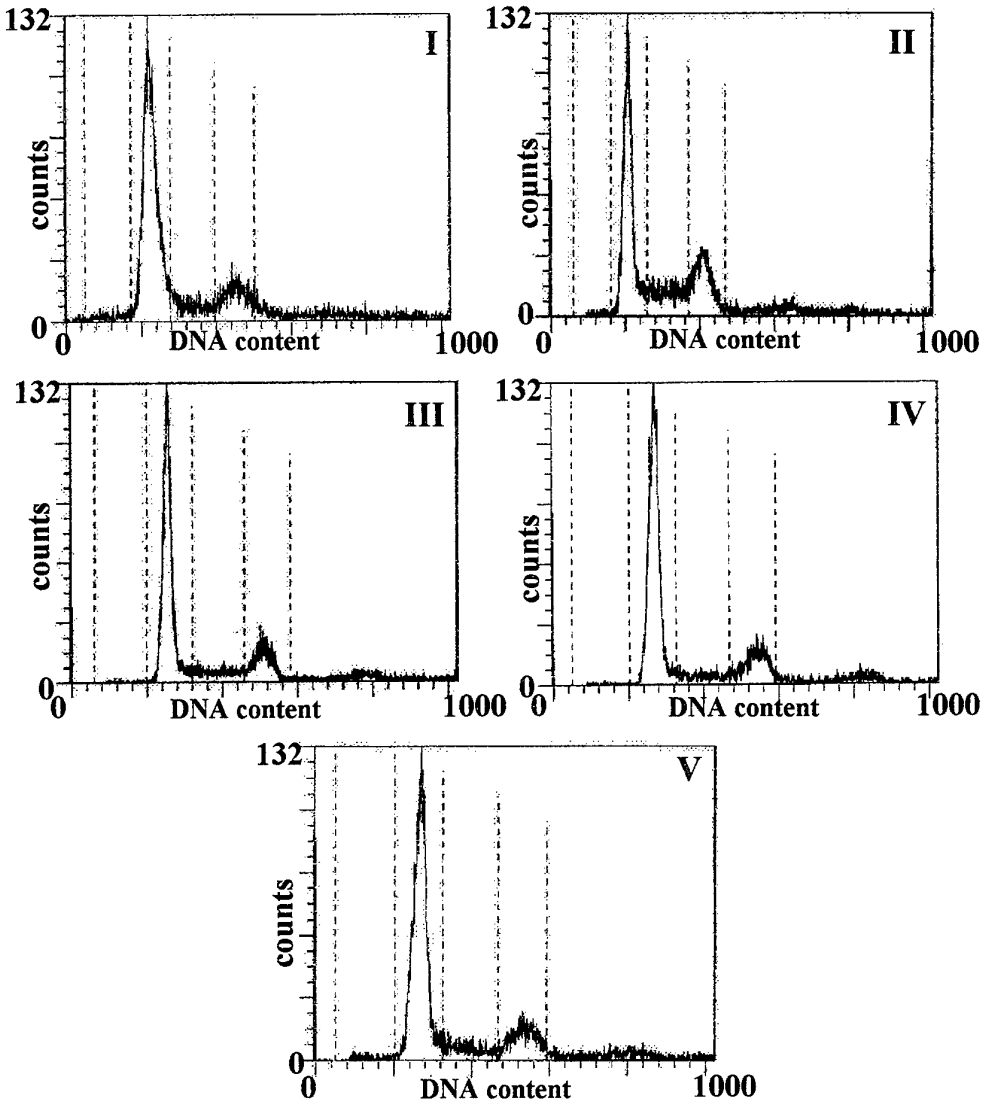

I – MDA-MB231:	**G0/G1 – 70.1%**	**S – 12.1%**	**G2/M – 17.4%**
II – MDA-MB435:	**G0/G1 – 62.9%**	**S – 17.2%**	**G2/M – 19.9%**
III – MCF7/LCC2:	**G0/G1 – 74.4%**	**S – 8.4%**	**G2/M - 17.2%**
IV – MCF7/MIII:	**G0/G1 – 72.9%**	**S – 7.9%**	**G2/M – 19.2%**
V – MCF7:	**G0/G1 – 72.7%**	**S – 9.8%**	**G2/M – 17.5%**

Figure 3. Cell cycle distribution of different cell lines. Cells grown as monolayer were incubated at 37°C and harvested before reaching confluence. The cell cycle phase-distribution was analyzed by FACS.

(ii) Growth Curves in Matrigel and Effects of Hormones

In order to determine the nature of the growth of these cell lines in Matrigel, a series of experiments were carried out in which cells were counted. The use of Matrigel caused problems with automatic counting due to clumping of the cells, and the lack of complete degradation of Matrigel by Dispase. Ultimately, a commercial mixture of Dispase and collagenase (Matrisperse) was found to work satisfactorily. The cells were counted manually. Growth curves of all cells were determined (**Fig. 4**). It can be seen that all the cells present exponential growth patterns. The doubling times obtained in Matrigel threads were comparable with those obtained for monolayers (**Table 2**); also inside Matrigel threads the doubling times were somewhat longer

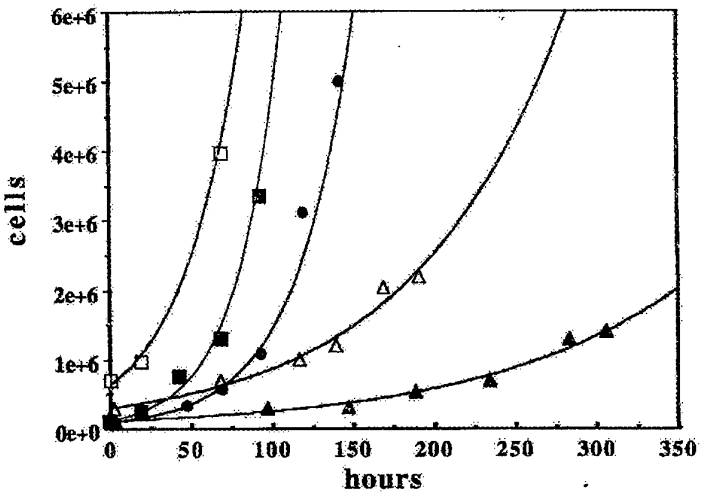

Figure 4. Growth curves of the cell lines in Matrigel. Cells were embedded in Matrigel and were incubated at 37°C. At the specified time points, the threads were dissolved by MatriSperse and cells were counted. MDA-MB231 (■); MDA-MB435 (□); LCC2 (▲); MIII (Δ); MCF7 (●). Lines fit have greater than 0.9R confidence factor.

Table 2. Doubling time of cell lines incubated at 37°C as monolayer.

Cell line	Doubling time
MDA-MB231	24 hr
MDA-MB435	23 hr
LCC2	65 hr
MIII	70 hr
MCF7	30 hr

The effects of estrogen (1 nM) on the growth rate of LCC2 cell line (estrogen responsive, Tamoxifen resistant) and of estrogen (1 nM) and Tamoxifen (5 μM) on the growth rate of MIII cell line (estrogen and Tamoxifen responsive) were determined (**Fig. 5**). Upon treatment of the cell lines with these hormonal effectors the growth curves were not found to be significantly changed. As a consequence no further hormonal growth studies were carried out with these cell lines.

(iii)^{31}P MR Spectra of Breast Cancer Cell Lines:

In previous ^{31}P MR studies, spectra of cell lines were obtained in perfused *agarose* gel threads (Ruiz-Cabello et al, 1994). Cells were routinely perfused for periods from 2 to 12 hours. It was not possible to see any effects of cell proliferation in agarose gel threads. Therefore, we grew the cells in *Matrigel* threads starting a low density, and were able to directly observe the increase in ^{31}P MR signals as the cells proliferated over 72 hr (**Fig. 6**). Note that the signal intensities increase in parallel and reach a plateau due to the effects of high density, consistent with Gompertzian growth. Note that the apparent decrease in the Pi signal probably arises from the dilution of the extra-cellular Pi as the extra-cellular volume decreases (Pi the only phosphate component that is extra-cellular).

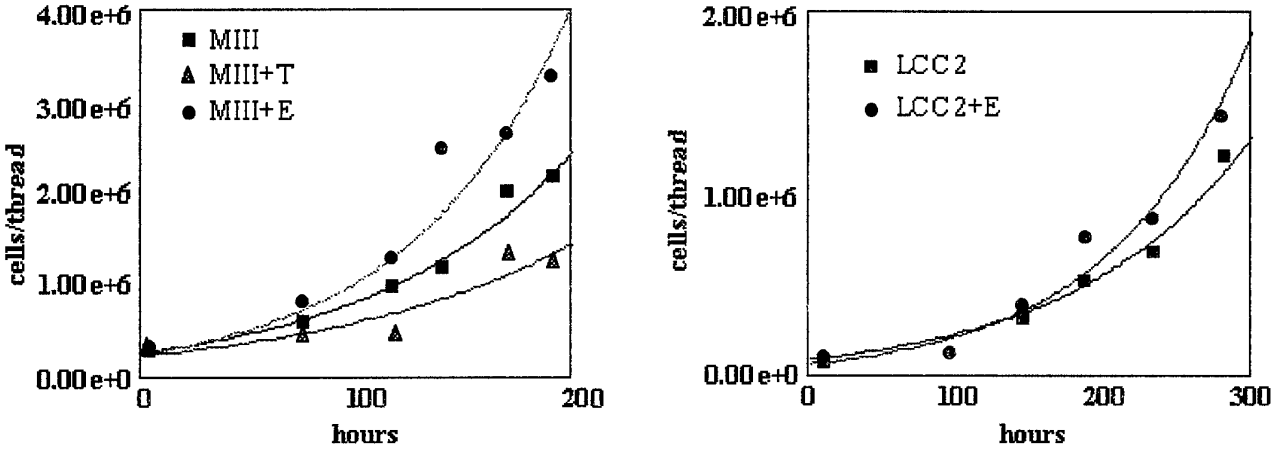

Figure 5. The effect of estrogen and Tamoxifen on cell growth in Matrigel. LCC2 and MIII cell lines were exposed to 1 nM estrogen (E). MIII was also exposed to 5 μM Tamoxifen (T). Cells were embedded in Matrigel and were incubated at 37°C. At the specified time points, the threads were dissolved by MatriSperse and cells were counted. Lines fit have greater than 0.9R confidence factor.

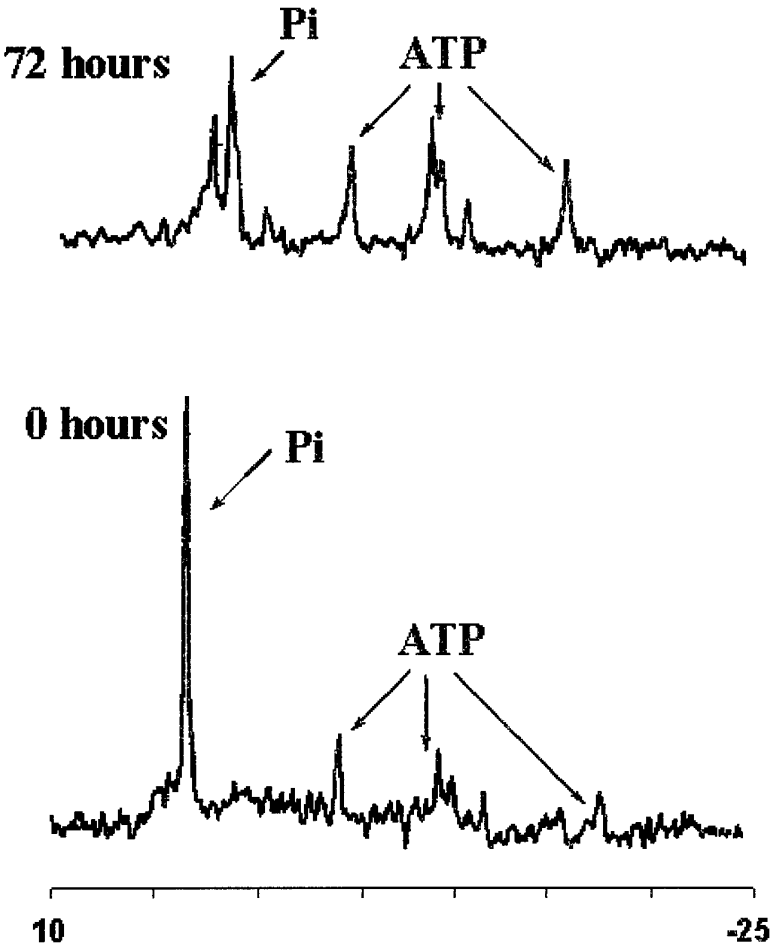

Figure 6. Viability and proliferation of cells embedded in Matrigel in an MRS perfusion system. MCF7 cells embedded in Matrigel were placed in perfused MRS tube. The changes in the ^{31}P spectrum during 72 hours of perfusion were recorded.

^{31}P MRS steady state spectra have now been obtained for five of the six cell lines listed in **Table 1** perfused in *Matrigel*. The cell line LY2 could not be grown satisfactorily during the period these experiments were underway. The ^{31}P MR spectra of each of these cell lines perfused in Matrigel are shown in **Fig. 7**. The integrals of the resolved and assigned peaks normalized to the β-ATP peak are given in **Fig 8**.

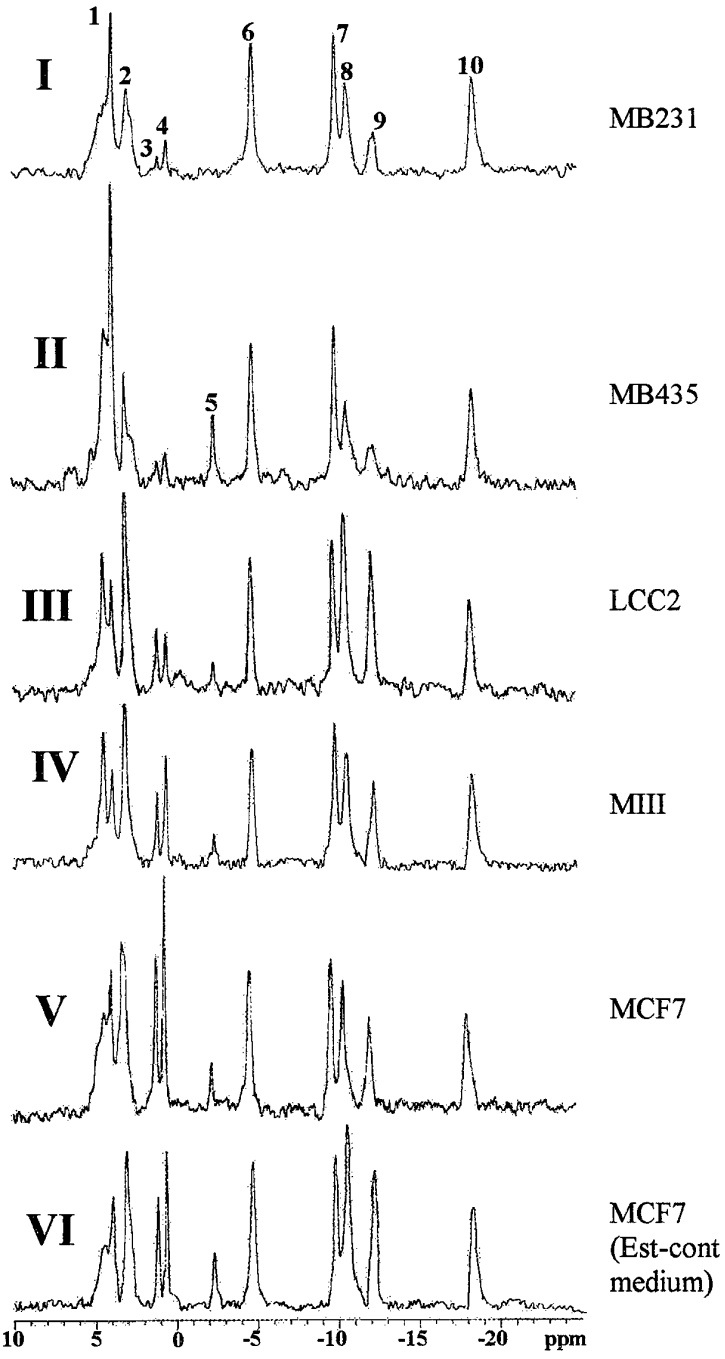

Figure 7. Comparison between the ^{31}P spectra of cell lines embedded in Matrigel threads. For this particular experiment, all cell lines (I-V) were perfused in the same medium (DMEM without phenol red, supplemented with charcoal stripped fetal calf serum) except for (VI) the spectrum of MCF7 cell line perfused in DMEM with phenol red, supplemented with estrogen-containing fetal calf serum. Assignments of the signals are: 1, PM; 2,Pi; 3, GPE; 4, GPC; 5, PCr; 6, γ-ATP; 7, α-ATP; 8, UDPS&NADP; 9, UDPS;10, β-ATP.

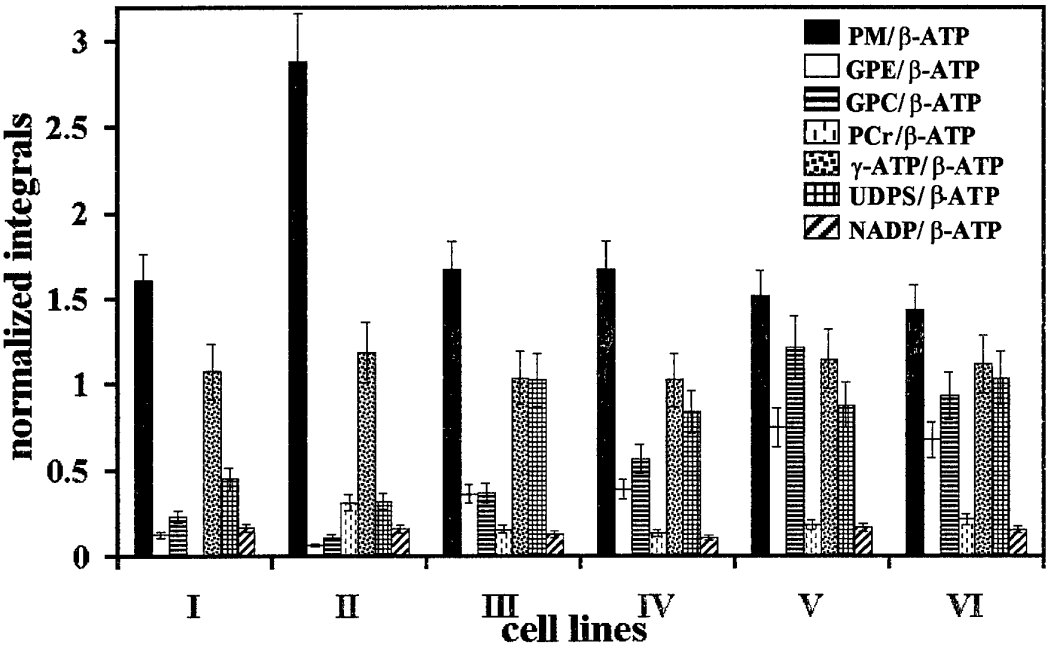

Figure 8. Intensities of ^{31}P MRS signals. The intensities of signals from the spectra in Figure 7 (cell lines as as in Fig. 7). Signal areas are normalized to the β-ATP peak in each spectrum.

It should be noted that there are significant differences in these spectra, which constitute a "fingerprint" of the metabolic state of the given cell line. Specific large differences in metabolite levels might be considered related to the differences in their hormonal properties. Analysis of the previous results obtained in agarose gel threads associated higher levels of PDE and UDPG and lower PC/GPC and PC/PE ratios with the acquisition of hormone independent status (Ruiz-Cabello et al, 1994). The results obtained in this study using Matrigel threads are somewhat different, depending on the level of glucose used in the perfusion medium. The most significant difference seen between the spectra is a much higher UDPS signal (peak 9) in ER^+ lines (LCC2, MIII and MCF7). Another significant difference is relatively low phospho-diester levels (GPE and GPC, peaks 3 and 4) in ER^+ lines (MIII and MCF7) as compared to ER^- MDA-MB231 and MDA-MB435 lines. The level of GPC is not significantly higher in the ER^+ LCC2 line as compared to the ER^- MDA/MB-231 line; however LCC2 has a significantly higher GPE level. It should be noticed that the PM level (peak 1) is higher in the MDA-MB435 line, which has higher metastatic potential then the other cell lines. The PCr level could not be associated with hormonal or metastatic status as it is non-visible in ER^- MDA- MB231cells, but visible (and relatively high) in the other ER^- line MDA-MB435. It is also visible in all the ER^+ lines. The tendencies that could be seen in the progression from lines representing an early type of breast cancer (estrogen-dependent, non-invasive MCF7) to more aggressive cell lines (estrogen responsive, estrogen-independent and Tamoxifen-sensitive MIII and estrogen-responsive, estrogen-independent and Tamoxifen-resistant LCC2) is a gradual decrease in the phospho-diester signals (GPE and GPC - peaks 3 and 4). Spectrum V shows the spectrum of the MCF7 line incubated for 3 days in an estrogen-free environment (medium without Phenol Red, charcoal stripped fetal calf serum), in which conditions the MCF7 line is not proliferating. Some decrease in UDPS and phospho-diester (GPE and GPC) levels can be seen in the estrogen-free conditions.

The levels of some metabolites were dependent on the glucose concentration in the culture medium. After 8 days of culture in medium with low glucose (11 mM) concentration almost all lines (except MDA-MB231) showed a significant decrease in the UDPS level. This could be expected, as the components of the UDPS peak are all glucose metabolites. In these conditions, as in high glucose (25 mM) conditions, the phospho-diester levels (peaks 3 and 4) are lower (actually invisible) in ER^- lines (MDA-MB231 and MDA-MB435) as compared with ER^+ lines. The differences seen in UDPS and diphosphodiester levels between ER^+ lines in high glucose conditions become less significant in low glucose conditions. The ER^+ but estrogen-independent MIII and LCC2 lines showed no PCr in their spectrum as opposed to the estrogen-dependent MCF7 line. No significant difference was observed for the MCF7 line between proliferative (spectrum VI) and non-proliferative estrogen-free conditions (spectrum V).

In conclusion, spectra of cell lines with different hormonal, metastatic and drug response status showed differences composing a "finger print" of the cell line. Higher UDPS and phospho-diester levels were seen in ER^+ lines. Levels of some metabolites (mostly UDPS and phosphodiesters) were dependent on glucose concentration in the culture medium. The decrease in phospho-diester levels on acquiring estrogen-independence and Tamoxifen-resistance in ER^+ lines was observed only in high glucose (25 mM) conditions. The difference in UDPS level between ER^+ and ER^- lines was observed only in low glucose (11 mM) conditions. However, differences in phospho-diester levels (GPE and GPC) between ER^+ and ER^- lines were observed in both high and low glucose culture conditions.

(iv) Assignment of Diphosphodiester Signals:

A significant difference in the diphosphodiester region of the ^{31}P MR spectrum (peak 9 in **Fig. 7**) was observed in the baseline spectra of the cell lines. The peak was high in the ER positive LCC2, MIII and MCF7 cells, but it was lower in ER negative MDA-MB231 and especially in MDA-MB435 cells. The peak is listed as UDPS in **Figure 8**, since the nature of the sugar component is unknown. To assign the peaks responsible for the difference, extraction with perchloric acid was performed as described above. Spectra of extracts enabled us to resolve the different compounds in the UDPS area because of the reduced line width. The peaks were assigned by spiking a sample with known compounds and were found to be N-acetyl-glucosamine (major component) and N-acetyl-galactosamine (minor component). The assignment of the UDPS area in LCC2 is shown in **Figure 9**. This pattern is the same in the other cell lines.

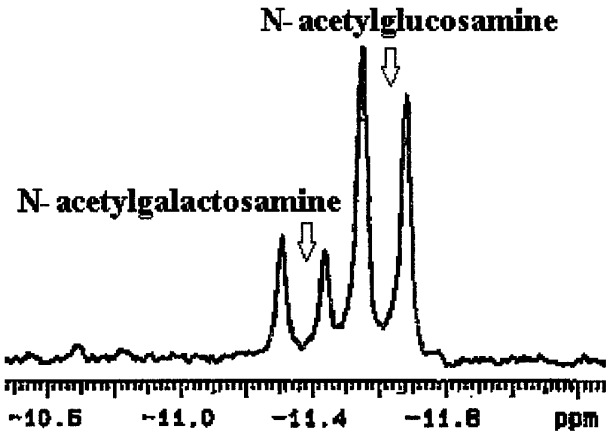

Figure 9. UDPS region in the spectrum of LCC2 cells. (Signal 9 in Fig. 7). The spectrum of a PCA extract is shown; the peaks were identified by spiking with authentic samples.

(v) Effects of Taxol

To insure adequate penetration of hydrophobic drugs into the Matrigel threads and the cells embedded in the threads, an experiment using radioactive ^3H-Taxol was performed as described in the Experimental Methods. Drug concentration was elevated with time in the threads and was increased (by a factor of 2) in threads loaded with cells, indicating drug accumulation inside the cells, until a plateau was achieved at 3 hours. **Figure 10** shows drug accumulation in bare threads and in threads loaded with cells. The absolute amount of radioactive drug per cell was checked for 3 situations. As a control, cells growing as a monolayer on plastic dishes were treated with ^3H-Taxol. Here nothing disturbs the penetration of ^3H-Taxol into the cells. As an additional control, cells were preloaded with the radioactive drug before their embedding in Matrigel and the threads were extruded into a dish containing medium with the radioactive drug. In this case cells would be saturated with the drug at the plateau value even if the Matrigel diminishes the penetration. To check the influence of Matrigel on the drug, the same procedure without the 1 hr preloading was performed (see Experimental Methods section). If the drug penetration is disturbed by Matrigel, the amount of radioactivity in the cells, which were not preloaded with the drug would be lower than for preloaded cells or cells growing as monolayer. In fact, the amount was similar with and without preloading and for the monolayer (2.1±0.2 cpm/1000cells). These results show that embedding cells in Matrigel threads does not prevent drug penetration inside the cells.

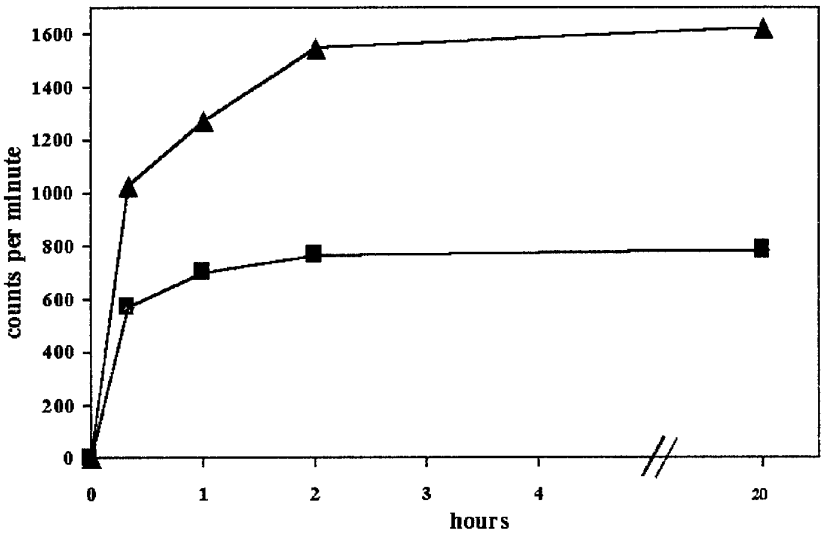

Figure 10. Uptake of Taxol in cells embedded in Matrigel threads. Threads with (▲) or without (■) MDA-MB231 cells, were immersed in medium containing 5 μM ^{3}H-Taxol. The threads were dissolved in tissue solubilizer and counted in a β-counter.

To decide on working concentrations of drugs for Matrigel experiments, the ED50 of Taxol in MDA-MB231 cell line embedded in Matrigel threads was compared to that for cells grown as monolayer. Cells (embedded in Matrigel threads or plated on 24 wells dish) were incubated with different concentrations of Taxol for 48 hours. After the incubation the cells embedded in Matrigel threads were liberated by MatriSperse and counted in a hemocytometer camera. Cells growing on dishes were harvested by trypsinisation and counted in a Coulter counter. The results are presented in **Figure 11**. It can be seen that the ED50 in Matrigel is higher by an order of magnitude. As shown in the previous section, this cannot be explained as a perturbation of drug penetration by Matrigel. Obviously the components of Matrigel or the experimental conditions have some protective action on cells. Consequently the concentration chosen for work with MDA-MB231 cells in Matrigel was $2.5x10^{-7}$M.

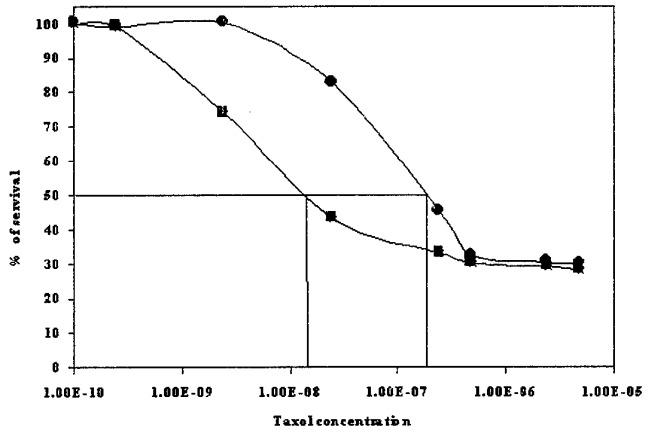

Figure 11. The effect of Taxol on the survival of MDA-MB231. MDA-MB231 cells, embedded in Matrigel threads (●) or grown as monolayer on plastic dishes (■), were exposed to a range of Taxol concentrations and incubated at 37°C. The cells were counted 48 hours later.

The effect was determined of different Taxol concentrations ($2.5x10^{-8}$ M and $2.5x10^{-7}$ M) on the cell cycle distribution of the cell lines under study embedded in Matrigel. It can be seen (**Fig. 12**) that the expected effects of Taxol – induction of apoptosis and of G2/M arrest – are achieved for all cells by the higher concentration ($2.5x10^{-7}$M). Consequently this concentration was chosen for work with all the cell lines. Even higher concentration was tried when no effect was seen. The cells were counted at the time of the experiment and the number of cells in the treated group was never lower then 40% of control.

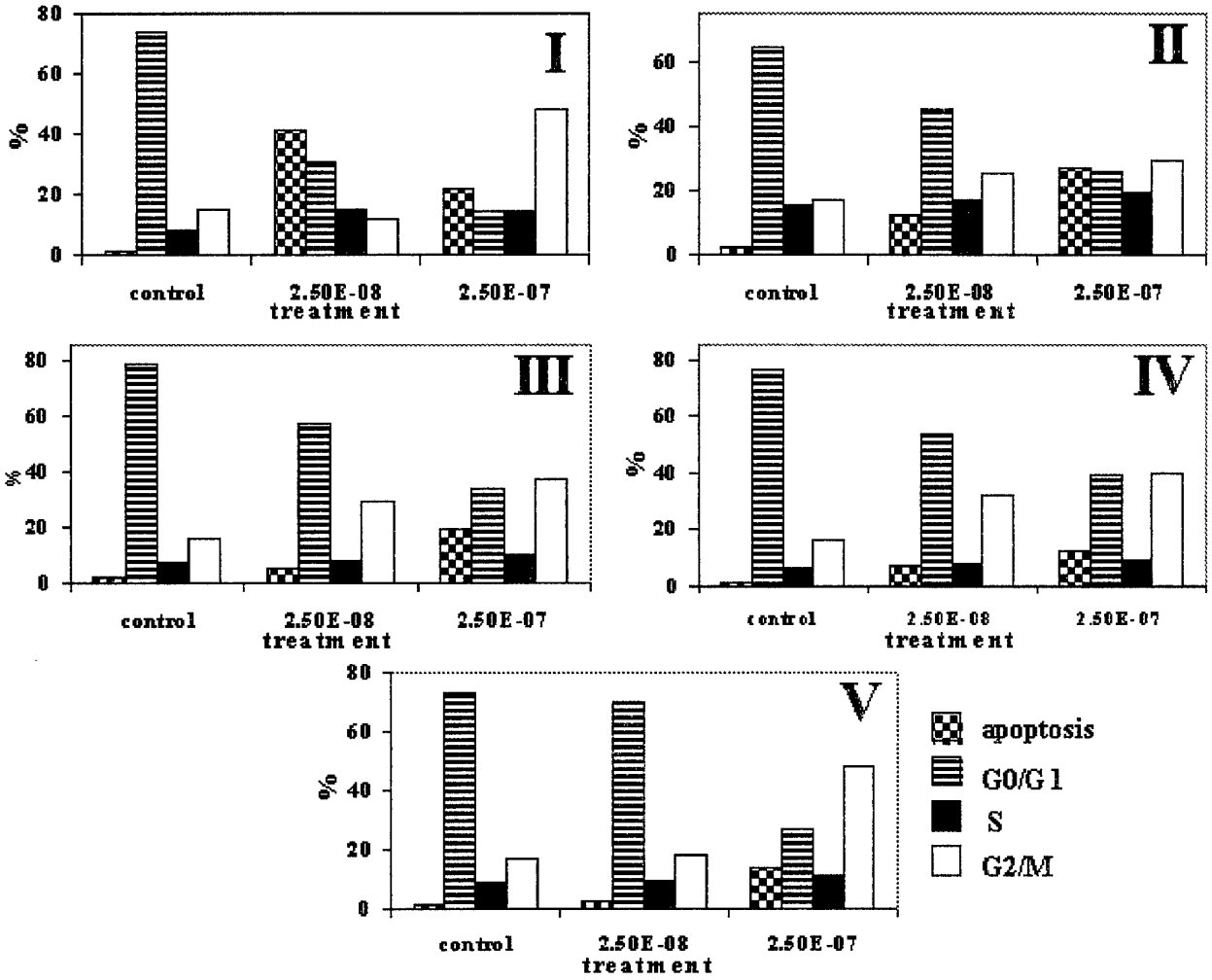

Figure 12. The effect of Taxol concentration on cell cycle distribution. MDA-MB231 (I), MDA-MB435 (II), LCC2 (III), MIII (IV), MCF7 (V) cell lines were treated with $2.5x10^{-7}$M and $2.5x10^{-8}$M Taxol for 48 hours. Cell cycle distribution was analyzed by FACS.

A time-course experiment treating MDA-MB231cells with $2.5x10^{-7}$ M Taxol was performed. Spectra were taken at several time points through 48 hr. The same procedure (preloading with DMSO 0.1%) was performed for control. It can be seen (**Figure 13**) that in both cases the GPC and PM peaks are elevated during the experiment, but in the Taxol-treated cells the elevation of GPC was much more profound. Elevation of PM and GPC in control cells is probably characteristic for cells growing in Matrigel. Elevation of PM in proliferating cancer cells was reported previously (Ruiz-Cabello and Cohen, 1992). This was checked by extracting cells growing as monolayer with and without trypsinisation so that GPC and PM are not diminished during harvesting with trypsin. Taxol treatment also lead to G2/M arrest and apoptosis. Since Taxol is acting mainly on cells in G2/M phase, it was hypothesized that the effect will be even more profound if cells will be treated with Taxol after they are synchronized in G2/M phase.

(vi) Synchronization Experiments and Effects of Drugs

Since Taxol is acting mainly on cells in G2/M phase, it was hypothesized that the effect will be even more profound if cells will be treated with Taxol after they are synchronized in G2/M phase. Cells were synchronized while growing in the dishes, washed, checked for the degree of synchronization, preloaded with Taxol, and then threads were prepared as for the Taxol treatment without synchronization, and time-course experiments were performed (as can be seen in **Fig. 14** synchronization with Nocodazole is reversible). The final result was very similar to that obtained with Taxol treatment alone. Thus, synchronizing the cells in G2/M stage did not increase the Taxol effect. Nevertheless the initial amount of GPC (0 hr) was higher in cells synchronized before Taxol treatment and GPC reached its final values during a shorter period of time (compare spectra after 3 hours in control, Taxol treated non-synchronized and Taxol-treated synchronized cells in **Figure 13**). This brought us to suggest that effect caused both by Taxol and by Nocodazole is responsible for GPC elevation. Both those drugs affect microtubules, cause G2/M arrest and may cause apoptosis.

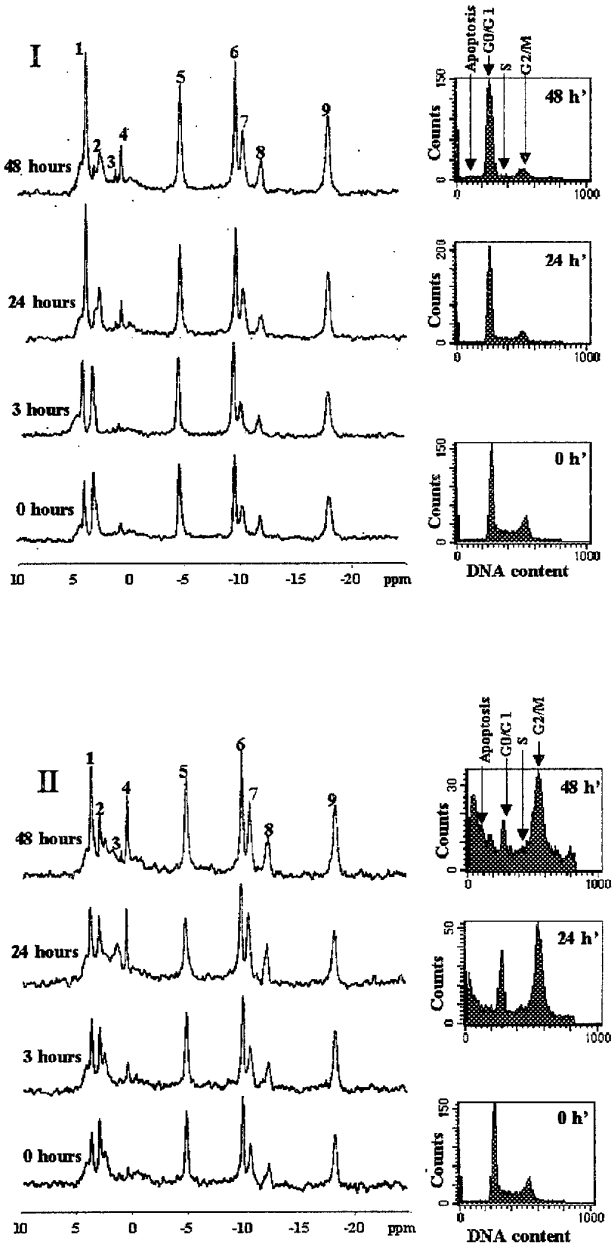

(for legend see next page)

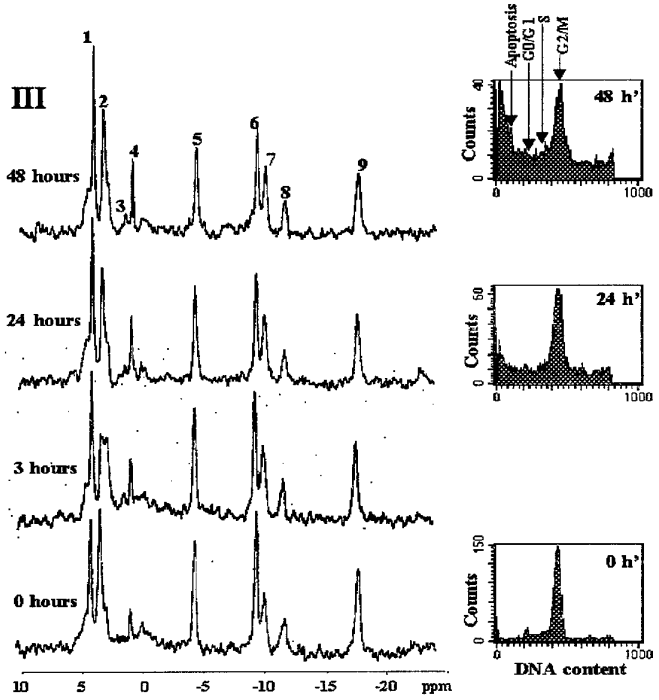

Figure 13. Spectra and cell cycle distribution of MDA-MB231 cells during MRS experiment. **I** - cells perfused with medium containing 0.1% DMSO; **II** – cells perfused in the presence of $2.5x10^{-7}$ M Taxol; **III** – cells perfused in the presence of $2.5x10^{-7}$ M Taxol after synchronization in G2/M by Nocodazole. Assignments of signals are:1, PM; 2,Pi; 3, GPE; 4, GPC; 5, γ-ATP; 6, α-ATP; 7, UDPS & NADP; 8, UDPS; 9, β-ATP.

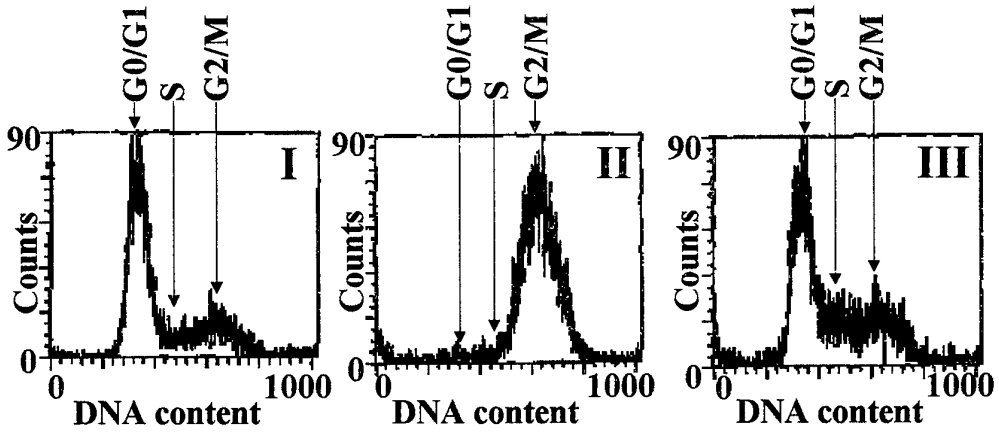

Figure 14. Effect of Nocodazole on cell cycle distribution of MDA-MB231 cells. MDA-MB231 cells were incubated for 12 hours without (I) and with (II) $3.3x10^{-7}$ M Nocodazole. (III) after 48 hr recovery from the same Nocodazole treatment.

The rise in the GPC level was shown to be a concentration effect and not due to a change in GPC relaxation times, possibly from transport of GPC to another cell compartment. Neither was it due to phospholipid head groups, since the cells were extracted with perchloric acid (PCA) after the ex vivo MRS experiments and phospholipids are not extracted by PCA. The spectra of the PCA extracts are presented in **Figure 15**. The results confirm the *ex vivo* results, showing that the change in GPC was absolute.

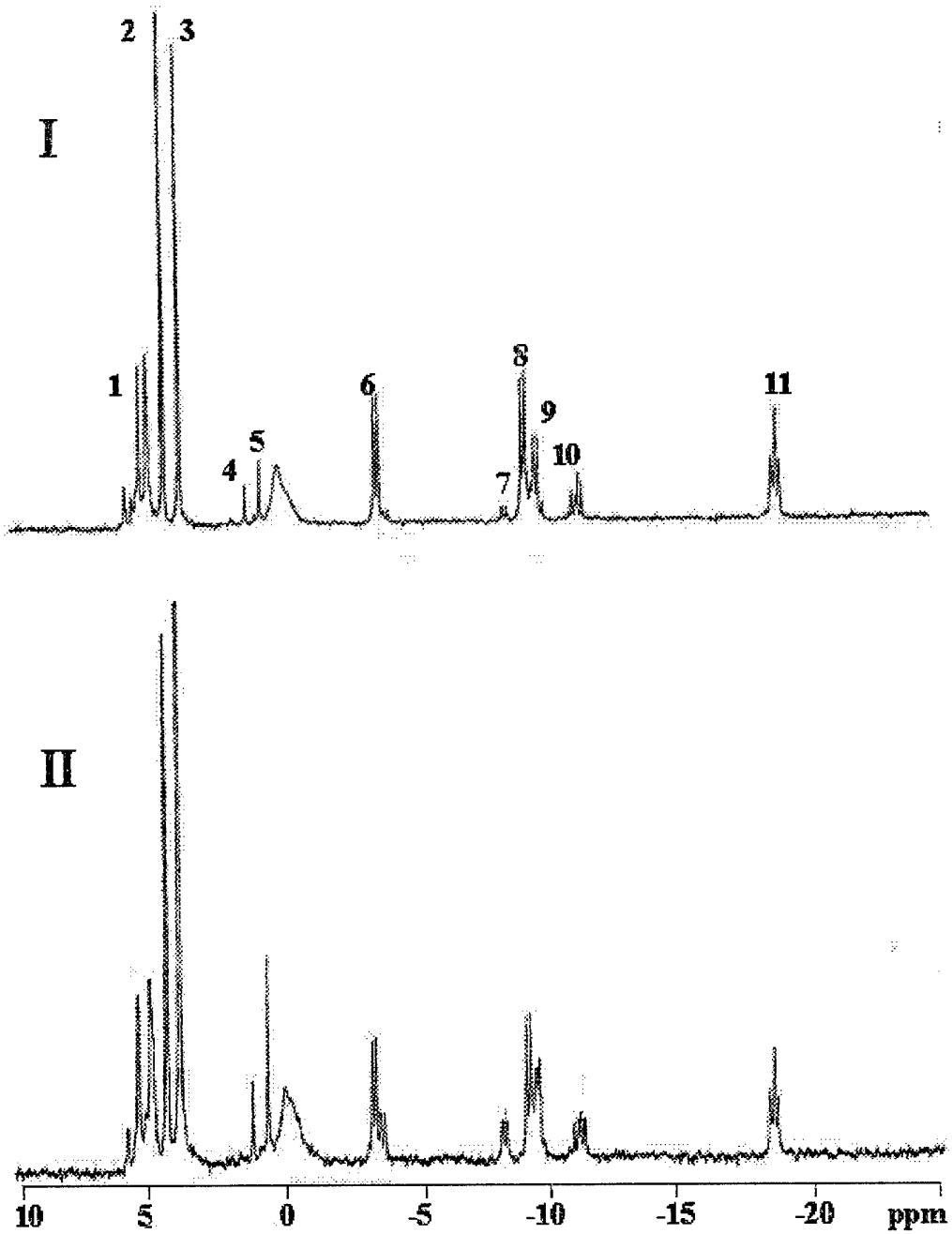

Figure 15. ^{31}P MRS spectra of perchloric acid extracts of cells after *ex vivo* experiments: MDA-MB231 cells embedded in Matrigel threads were perfused in MRS system for 48 hours with medium containing 0.1% DMSO (I) or in the presence of $2.5x10^{-7}$ M Taxol. After completion of the experiments the cell content was extracted by perchloric acid and analyzed by ^{31}P MRS. Assignments of signals are:1, PM; 2, PC; 3, Pi; 4, GPE; 5, GPC; 6, γ-ATP; 7, β-ADP; 8, α-ADP; 9, α-ATP; 10, UDPS & NADP; 11, β-ATP.

To assure that the GPC rise was not specific for cells embedded in Matrigel an experiment with MDA-MB231 cells embedded in alginate capsules was performed. The GPC rise in Taxol-treated cells relative to control was also observed in this system. The GPC signal was shown to be intra-cellular by performing the experiment for cells growing on dishes, removing the dead cells by aspiration, and extracting with PCA the remaining viable cells (98% by trypan blue exclusion). The rise in GPC was also seen in this experiment. To assure that the GPC rise in the *ex vivo* MRS experiment was not due to release of GPC into the medium from disrupted cells the supernatant medium was collected and checked by MRS and the only signal seen was that of Pi.

(vii) Effects of Drugs on GPC Levels in ^{31}P MR Spectra of Cells

To clarify the cause of the GPC rise with Taxol, several experiments with other drugs were performed using the more convenient end-point method. Drug concentrations were chosen to be about 10 times ED50 for MDA-MB231 cells growing as a monolayer. An even higher concentration was tried when no effect was seen. The cells were counted at the time of the experiment and the number of cells in the treated set was never lower then 40% of control. Regarding apoptosis, interestingly, $2.5x10^{-8}$ M of Taxol caused more apoptosis than $2.5x10^{-7}$ M in MDA-MB231 cells (**Figure 12**). Nevertheless, GPC rise was seen after treatment with $2.5x10^{-7}$ M but not with $2.5x10^{-8}$ M (results not shown), so apoptosis probably does not explain the rise in GPC.

As to G2/M arrest and action on microtubules, the issue was studied by treating the MDA-MB231 cells with different drugs (end-point method). The cells were treated in this manner with Taxol ($2.5x10^{-7}$ M, 48 hr), with Nocodazole ($3.3x10^{-7}$ M, 24 hr), with Vincristine ($3x10^{-7}$ M, 48 hr), with Colchicine ($2.5x10^{-7}$ M, 24 hr), with Adriamycin ($1.2x10^{-6}$ M, 48 hr) and with Methotrexate ($1.1x10^{-5}$ M, 48 hr). It should be noted that MDA-MB231 cells are resistant to Methotrexate but at the high concentrations used here an effect might have be seen. From **Figure 16** it is clearly evident that while anti-microtubule drugs (Taxol, Nocodazole, Vincristine and Colchicine) enhance the concentration of intra-cellular GPC (relative to β-ATP) such an effect was not observed for the non-anti-microtubule active drugs (Adriamycin and Methotrexate). The MRS studies were accompanied by cell cycle studies. One thread was dissolved and the cycle the cells was determined by FACS after 24 hr of treatment and at the time of the experiment (if later). The results are presented in **Table 3**; it should be noted that Adriamycin causes G2/M arrest but no GPC rise, so that the increase in GPC probably is not caused by G2/M arrest.

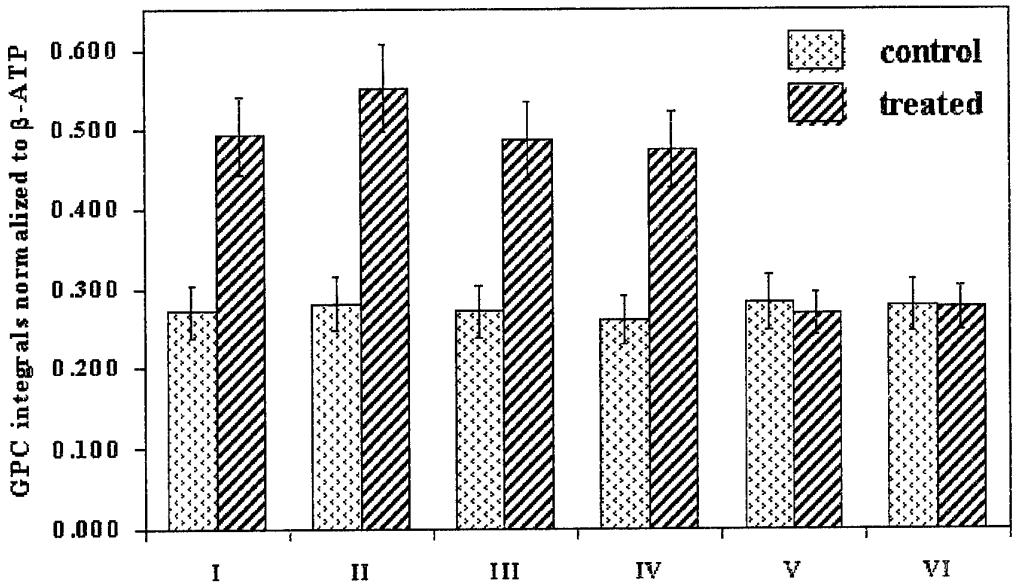

Figure 16. GPC content in control vs. treated MDA-MB231 cells: I - Taxol ($2.5x10^{-7}$ M, 48 hr), II - Nocodazole ($3.3x10^{-7}$ M, 24 hr), III - Vincristine ($3x10^{-7}$ M, 48 hr), IV - Colchicine ($2.5x10^{-7}$ M, 48 hr), V - Adriamycin ($1.2x10^{-6}$ M, 48 hr), VI - Methotrexate ($1.1x10^{-5}$ M, 48 hr).

It should be noted that further rise of Adriamycin concentration ($3.4 x10^{-6}$ M, 48 hr) did cause elevation of GPC. To clarify this point and to study more about the cause of GPC elevation by anti-microtubule drugs, phospholipid extracts were performed for cells treated with Taxol ($2.5x10^{-7}$ M, 48 hr) and with Adriamycin ($3.4 x10^{-6}$ M, 48 hr). It can be seen in **Figure 17** thatTaxol did not cause any significant effect on the phospholipid profile, so that the rise of intra-cellular GPC observed is probably due to decreased GPC degradation. A high concentration of Adriamycin A caused a significant effect on the phospholipid profile (Fig. 17, mainly decrease of PtdC comparatively to other components and especially increase of Plasm PtdC comparatively to PtdC). Thus, the elevation of GPC observed is due to cell membrane degradation.

Table 3. Cell cycle distribution of MDA-MB231 cells treated with drugs: I - Taxol, II - Nocodazole, III - Vincristine, IV - Colchicine, V – Adriamycin, and VI - Methotrexate. Concentrations are as in Figure 16. (N.D., not determined).

Phase	Control	I	II	III	IV	V	VI
24 hours							
Apoptosis	1.7±0.8	10.4±5.4	9.7±3.6	10.2±0.5	9.1±2.2	2.0±1.5	1.7±0.9
G0/G1	67.9±3.7	19.5±4.0	16.3±3.5	19.6±7.6	24.4±4.3	25.3±4.9	74.6±1.7
S	11.8±3.3	13.0±4.5	11.7±2.8	15.2±0.6	18.0±1.4	7.0±2.1	7.1±1.4
G2/M	18.8±3.3	57.0±6.9	62.2±4.5	55.1±6.5	48.5±5.0	65.7±6.5	16.4±2.1
48 hours							
Apoptosis	1.7±0.8	22.1±5.0	N.D.	14.7±5.6	30.0±1.1	4.1±2.4	2.7±0.5
G0/G1	74.1±2.4	14.6±2.9	N.D.	23.3±5.5	14.4±3.4	17.1±5.5	76.6±0.9
S	8.1±1.0	14.8±3.1	N.D.	14.3±3.0	11.7±1.0	6.8±1.9	6.9±0.7
G2/M	16.1±1.7	48.2±7.4	N.D.	47.7±7.7	43.9±4.4	71.9±1.3	13.7±0.6

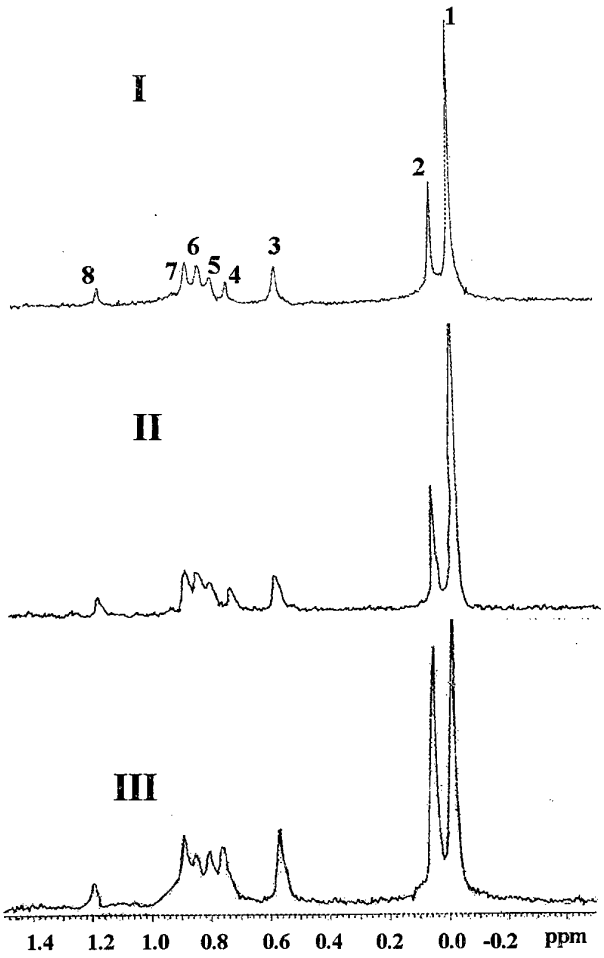

Figure 17. ^{31}P MRS spectra of phospholipid extracts of cells after drug treatment: MDA-MB231 cells were incubated for 48 hours (I) without, (II) with 2.5×10^{-7} M Taxol, or (III) with 3.4×10^{-6} M Adriamycin. Assignments for the signals are: 1, PtdC; 2, Plasm.PtdC; 3, PtdI; 4, SPH; 5, PtdS; 6, PtdE; 7, Plasm.PtdE; 8, cardiolipin).

The effects of the same drugs in the same concentrations were checked for other cell lines. A lower concentration of Methotrexate ($5X10^{-6}$ M) was used initially, as the MDA-MB231 line is resistant to this drug, and other cell lines are not. Higher concentrations (up to $1.1x10^{-5}$ M) were tried when no effect was seen. The cells were counted at the time of the experiment and number of cells in treated group was never lower then 40% of control.

The results for MDA-MB435 cells are shown in **Figure 18**. It can be seen that anti-microtubule drugs induce significant GPC elevation. The small GPC elevation caused by Adriamycin is probably due to membrane attack. The cell cycle results are shown in **Table 4**. The general effects on cell cycle are similar to those in MDA-MB231 cells – induction of apoptosis and G2/M arrest by anti-microtubule active drugs, G2/M arrest and some apoptosis by Adriamycin, some apoptosis and some G1 arrest by Methotrexate.

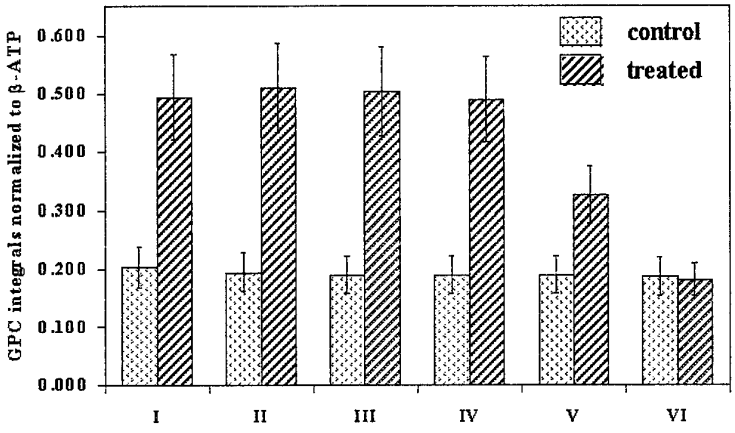

Figure 18. GPC content in control vs. treated MDA-MB435 cells: I - Taxol ($2.5x10^{-7}$ M, 48 hr), II - Nocodazole ($3.3x10^{-7}$ M, 24 hr), III - Vincristine ($3x10^{-7}$ M, 48 hr), IV - Colchicine ($2.5x10^{-7}$ M, 48 hr), V - Adriamycin ($1.2x10^{-6}$ M, 48 hr), VI - Methotrexate ($5x10^{-6}$ M, 48 hr).

Table 4. Cell cycle distribution of MDA-MB435 cells treated with drugs: I - Taxol, II - Nocodazole, III - Vincristine, IV - Colchicine, and V – Adriamycin, and VI - Methotrexate. Concentrations are as in Figure 18. (N.D., not determined).

Phase	Control	I	II	III	IV	V	VI
24 hours							
Apoptosis	1.7±0.8	10.4±5.4	9.7±3.6	10.2±0.5	9.1±2.2	2.0±1.5	1.7±0.9
G0/G1	67.9±3.7	19.5±4.0	16.3±3.5	19.6±7.6	24.4±4.3	25.3±4.9	74.6±1.7
S	11.8±3.3	13.0±4.5	11.7±2.8	15.2±0.6	18.0±1.4	7.0±2.1	7.1±1.4
G2/M	18.8±3.3	57.0±6.9	62.2±4.5	55.1±6.5	48.5±5.0	65.7±6.5	16.4±2.1
48 hours							
Apoptosis	1.7±0.8	22.1±5.0	N.D.	14.7±5.6	30.0±1.1	4.1±2.4	2.7±0.5
G0/G1	74.1±2.4	14.6±2.9	N.D.	23.3±5.5	14.4±3.4	17.1±5.5	76.6±0.9
S	8.1±1.0	14.8±3.1	N.D.	14.3±3.0	11.7±1.0	6.8±1.9	6.9±0.7
G2/M	16.1±1.7	48.2±7.4	N.D.	47.7±7.7	43.9±4.4	71.9±1.3	13.7±0.6

The results for MCF7 cells are shown in **Figure 19**. It can be seen that the GPC effects are insignificant. It should be noticed that treatment with Adriamycin (1.2×10^{-7} M and 3.4×10^{-7} M) caused increase of the PCr signal in this cell line. Increase in PCr was reported for Adriamycin-resistant MCF7 cells embedded in agarose threads (Cohen et al., 1986). MRS studies of Adriamycin sensitive and resistant MCF7 tumors grown in nude mice, following treatment with Adriamycin, showed an increase in PCr (and ATP) content for the sensitive but nor for the resistant tumors (Evelhoch et al, 1987). The cell cycle results for MCF7 are shown in **Table 5**. The general effects on cell cycle are similar to those for MDA-MB231 and MDA-MB435 cells.

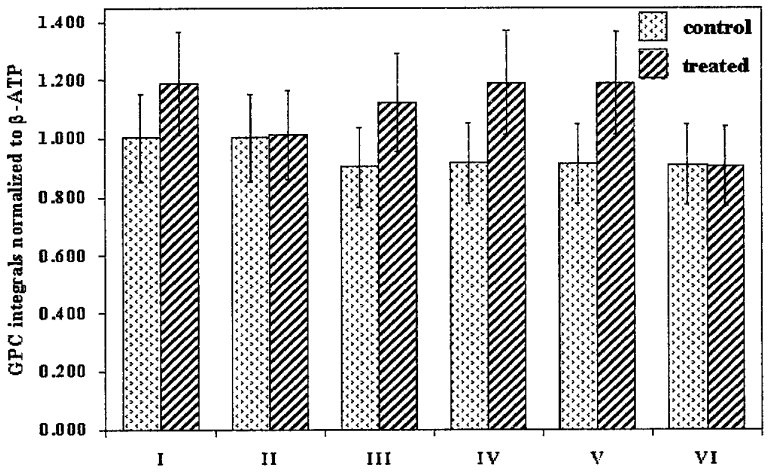

Figure 19. GPC content in control vs. treated MCF7 cells: I - Taxol (2.5×10^{-7} M, 48 hr), II - Nocodazole (3.3×10^{-7} M, 24 hr), III - Vincristine (3×10^{-7} M, 48 hr), IV - Colchicine (2.5×10^{-7} M, 48 hr), V - Adriamycin (1.2×10^{-6} M, 48 hr), VI - Methotrexate (5×10^{-6} M, 48 hr).

No effect on the phosphorus metabolites was seen after drug treatments of LCC2 and MIII cells. The cell cycle results are shown in **Table 6** for the LCC2 cell line, and in **Table 7** for MIII cells. The general effects on cell cycle are similar to those in MDA-MB231, MDA-MB435 and MCF7 cell lines. Less effect at 24 hours may be explained by longer doubling time of these cell lines.

Absence of effect of drug treatments on GPC levels in MCF7, LCC2 and MIII lines may be explained by their higher basic level of GPC or by the presence of estrogen receptors in these cells.

Table 5. Cell cycle distribution of MCF7 cells treated with drugs: I - Taxol, II - Nocodazole, III - Vincristine, IV - Colchicine, and V – Adriamycin, and VI - Methotrexate. Concentrations are as in Figure 19. (N.D., not determined).

Phase	Control	I	II	III	IV	V	VI
24 hours							
Apoptosis	1.7±0.6	6.0±2.2	6.6±2.2	5.0±1.4	6.0±1.4	8.0±4.2	5.3±0.6
G0/G1	68.0±3.6	18.5±3.2	17.0±4.1	36.0±7.1	35.0±4.2	52.0±4.8	68.7±1.5
S	11.7±2.9	18.0±4.2	11.3±1.1	11.5±2.1	11.5±2.1	9.5±2.1	8.3±2.3
G2/M	18.6±3.1	57.5±6.4	65.1±7.0	47.5±3.5	47.5±4.9	30.5±6.1	17.7±0.6
48 hours							
Apoptosis	1.2±1.0	13.7±2.1	N.D.	8.5±4.4	14.2±5.1	11.1±4.1	13.0±2.8
G0/G1	73.2±3.9	27.1±4.1	N.D.	27.5±5.1	22.7±6.0	41.7±3.1	61.0±9.2
S	9.0±1.4	11.0±2.4	N.D.	13.0±1.0	15.1±3.0	9.8±1.7	11.5±0.7
G2/M	16.6±2.8	48.2±5.1	N.D.	51.0±0.8	48.0±6.1	37.4±6.2	14.5±2.1

Table 6. Cell cycle distribution of LCC2 cells treated with drugs: I - Taxol, II - Nocodazole, III - Vincristine, IV - Colchicine, and V – Adriamycin, and VI - Methotrexate. Concentrations are as in Figure 19. (N.D., not determined).

Phase	Control	I	II	III	IV	V	VI
24 hours							
Apoptosis	1.3±0.5	8.8±3.2	9.5±2.5	8.4±5.1	10.6±2.7	2.5±1.9	7.0±2.3
G0/G1	73.5±2.7	59.9±4.8	37.5±4.1	57.8±6.1	61.2±6.0	70.2±2.8	68.2±3.1
S	8.0±1.2	8.6±1.4	8.7±1.9	8.1±2.1	6.9±1.0	6.8±0.8	8.1±0.9
G2/M	17.2±1.4	22.7±6.3	44.3±7.3	25.7±5.1	21.3±5.4	20.5±2.0	16.7±1.9
48 hours							
Apoptosis	2.2±1.1	19.3±6.5	N.D.	15.9±6.1	22.1±6.5	8.9±4.1	12.0±3.3
G0/G1	73.8±1.7	33.9±5.9	N.D.	50.7±4.6	48.2±6.9	59.8±3.1	61.9±2.7
S	7.3±1.1	9.7±0.8	N.D.	7.6±1.5	8.7±1.6	7.8±2.3	12.4±2.1
G2/M	16.7±2.8	37.1±6.3	N.D.	25.8±6.8	21.0±3.6	23.5±3.1	13.7±1.7

Table 7. Cell cycle distribution of MIII cells treated with drugs: I - Taxol, II - Nocodazole, III - Vincristine, IV - Colchicine, and V – Adriamycin, and VI - Methotrexate. Concentrations are as in Figure 19. (N.D., not determined).

Phase	Control	I	II	III	IV	V	VI
24 hours							
Apoptosis	1.9±0.6	7.4±4.1	7.9±3.3	6.5±3.5	10.7±4.5	5.3±1.9	2.0±0.7
G0/G1	76.7±2.3	60.4±4.5	35.5±4.1	71.6±4.1	66.8±5.1	70.9±2.5	76.9±2.9
S	6.2±2.7	7.2±1.3	7.1±1.4	4.1±2.2	4.1±1.3	5.9±1.7	6.7±1.3
G2/M	15.2±3.0	25.0±4.1	49.5±4.0	17.9±6.1	18.4±5.3	17.9±3.7	14.4±1.5
48 hours							
Apoptosis	1.2±0.3	12.5±5.1	N.D.	13.1±2.5	10.6±3.0	3.9±0.6	1.9±0.4
G0/G1	76.7±1.9	39.1±4.7	N.D.	40.3±3.1	36.5±4.0	65.6±1.9	77.5±1.5
S	6.2±0.8	8.7±3.1	N.D.	8.0±1.7	6.9±1.5	7.6±1.5	6.7±0.5
G2/M	15.9±1.6	39.7±4.9	N.D.	38.6±4.5	46±5.7	22.9±3.1	14.3±0.6

(viii) Proton DWMRS Studies of Breast Cancer Cell Lines

In order to prove that we are able to separate the intra/extra-cellular components, we plotted the attenuation curve for water as a function of the square of the gradient intensity (which is proportional to the diffusion-weighted factor **b**, equation 1) for perfused cells embedded in alginate beads. In the simplest case of a two-compartment system with very slow exchange between them, the attenuation of the water signal should be a bi-exponential function of **b**, with the small apparent diffusion coefficient (D) originating from the intra-cellular molecules and the high D arising from the combination of intra- and extra-cellular molecules. **Figure 20** shows a diffusion curve of perfused MCF7 human breast cancer cells embedded in alginate beads (diamonds), and of control beads without cells (rectangles). It can be seen that the perfused cells exhibit bi-exponential decay, with the fast decay component originating from the extra-cellular compartment, and the slow decay coming from both the extra- and intra-cellular components, which is missing in the case of the medium containing beads without cells.

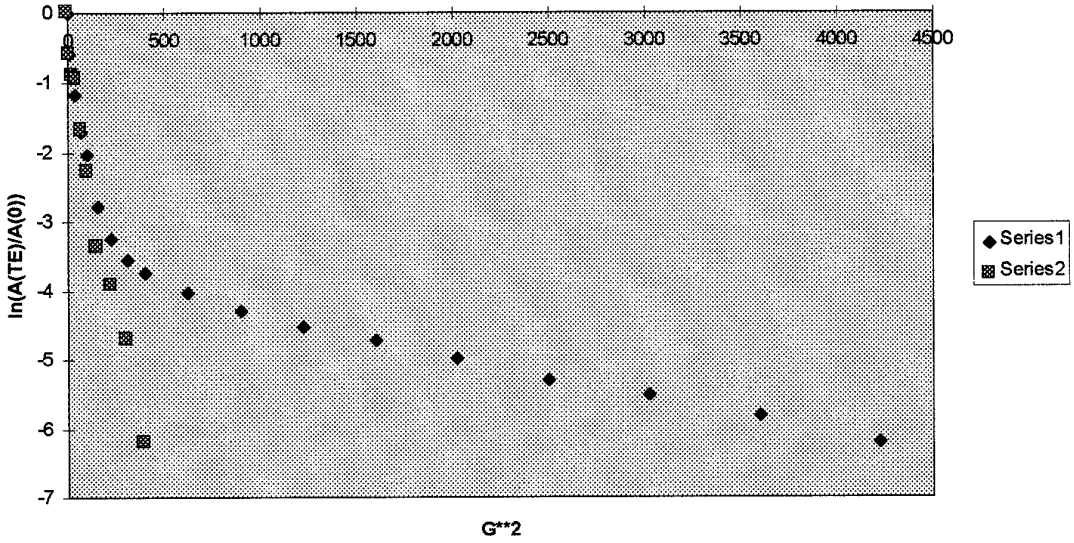

Figure 20. Normalized water proton signal attenuation as a function of square of gradient strength g^2 (in $[mT/m]^2$) for perfused MCF7 cells (diamonds) and of control gel (squares).

An additional test was performed by changing the extra-cellular medium to a buffer without any metabolites. For this purpose, we perfused the cells with PBS and showed that the intra-cellular spectrum did not change. **Figure 21** shows the perfusion of MCF7 cells with PBS, which was chosen since it shows no peaks in proton MRS (except for the water peak). Two types of MR sequences were used: the diffusion weighted sequence (described previously) which results in intra-cellular spectra (shown in the top plot of Fig. 21) and the pre-saturation sequence (which is a conventional spin echo sequence preceded by a special selective pulse which destroys the water signal) resulting in a spectrum which is a convolution of the intra- and extra-cellular peaks (middle and bottom plots of Fig. 21).

The top plot (**Fig. 21**) shows that there is no change in the intra-cellular spectrum when changing the perfusion from conventional medium to PBS, as expected. The middle plot shows the changes in the intra- plus extra-cellular spectra caused by this switch. It is possible to see that with time some of the peaks decrease in intensity or width and some disappear altogether. The bottom plot shows the pre-saturation (water suppressed) spectrum of the conventional perfusion medium. There is a clear correlation between the peaks in this spectrum and the peaks that disappeared from the spectra in the middle plot. Since the spectra of the top plot (intra-cellular) did not change when the medium was replaced by PBS, and the pre-saturation spectra of the cells (middle plot) did change (and these changes were correlated with the extra-cellular medium) we concluded that this test, as well as the double slope in the diffusion curve (**Fig. 20**) confirms that the diffusion weighted spectra are indeed intra-cellular.

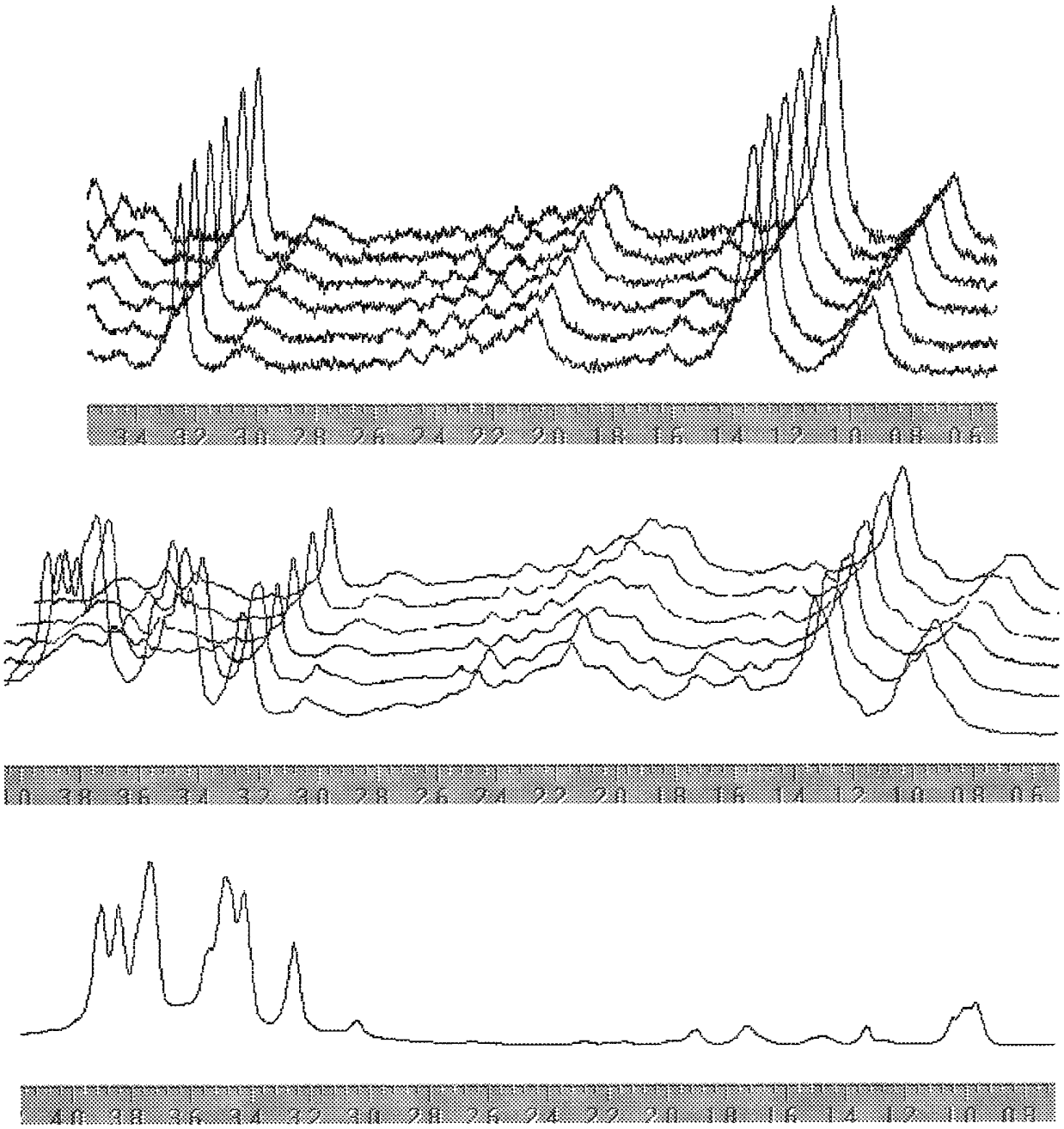

Figure 21. Perfusion of MCF7 cells with PBS. The top plot shows the diffusion weighted spectra (intra-cellular) of perfused cells, taken immediately after switching the perfusion medium to PBS, and then at 5 min intervals. The middle plot shows the pre-saturation spectra (intra- plus extra-cellular) of the same perfused cells. The bottom spectrum is the pre-saturation spectrum of the extra-cellular medium alone. See text for details.

We measured intra-cellular proton spectra of five human breast cancer cell lines using the DWMRS method. The intracellular spectra were obtained by choosing a gradient value in the region of the slow slope of the diffusion curve (**Fig. 20**), where the NMR signal obtained originates from slow moving molecules, i.e. intra-cellular molecules. Between three and five spectra were recorded for each cell line, at least one month apart. **Figure 22** shows an example of one spectrum taken for each cell line. By looking at the shapes of these spectra, it seems reasonable to divide them into three groups: the first group consists of the top three spectra – MCF7, MB231 and MB435, the second group consists of the next two spectra – LCC2 and MIII, and the third

is the melanoma cell line. The differences between the cell lines are described by ratios between peaks or regions of peaks in the spectra. For example, the ratio between the lactate region (1.2-1.5 ppm) and the choline area (3.2-3.4 ppm) is larger than 1.0 in the first group, smaller than 1.0 in the second group and close to 1.0 in the third. The same is true for the ratio between the lactate region and the region of leucine/isoleucine (0.8-1.0 ppm). Looking more carefully at the lactate region, one can see that there is also a difference between the groups in the fine structure of this region of the spectra. Also, the peaks in the 2-2.6 ppm region seem different, and the peak at 2-2.2 ppm seems to dominate in the second group.

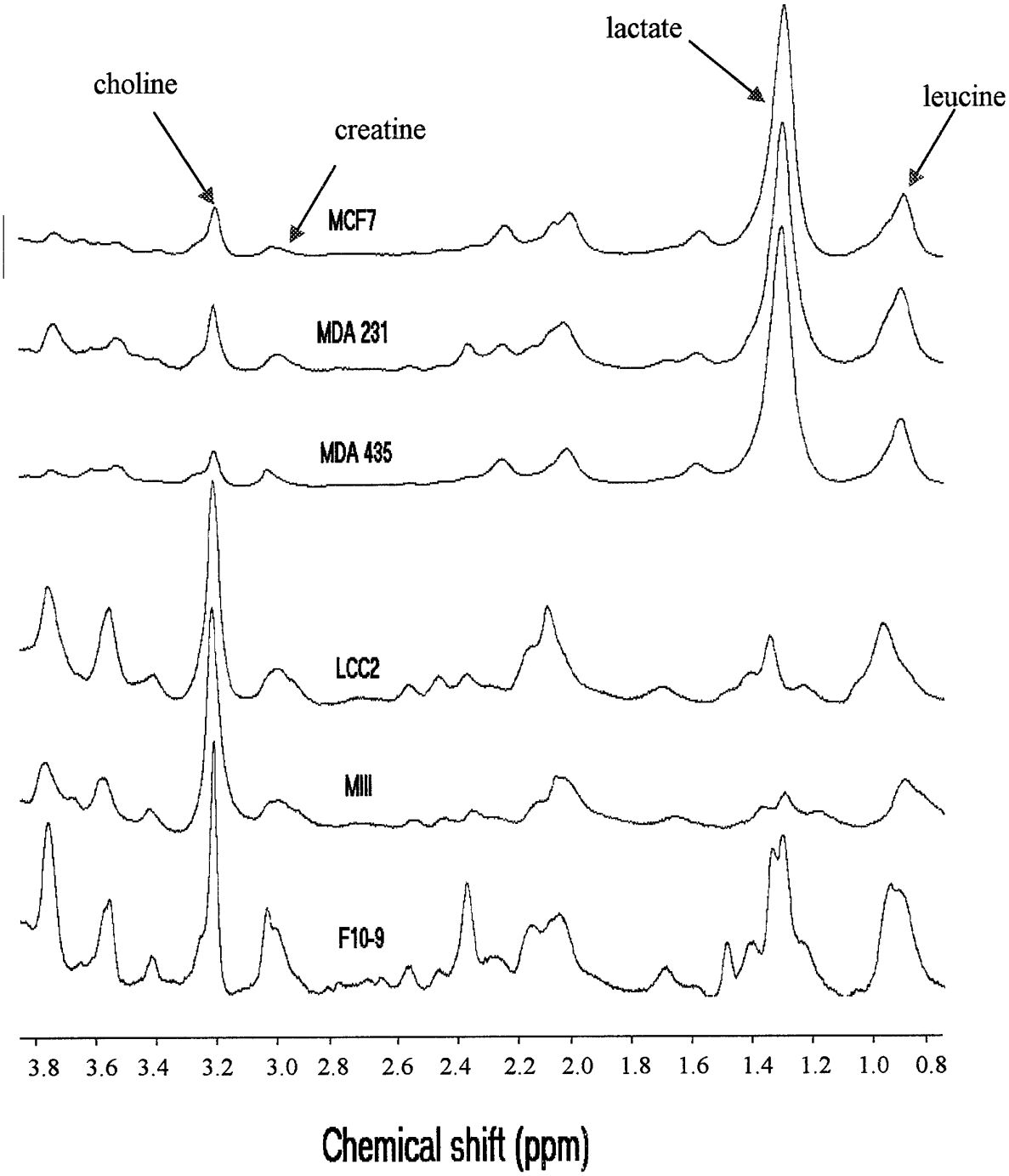

Figure 22. Qualitative comparison of ^{1}H MR intra-cellular spectra of breast cancer cell and of F10-9 melanoma cells.

In order to determine if there are any significant differences between the cell spectra it is necessary to be able to quantitate the analysis by fitting the signals with theoretical curves. Although MR signals are generally considered to have a Lorentzian line shape, in the case of broad signals from biological samples Gaussian curves are generally found to give better fits. This is presumably because of the presence of chemical shift heterogeneity due to heterogeneous environments that causes biological samples to give broader signals. **Figure 23** shows an example of a digitized spectrum taken for MCF7 cells.

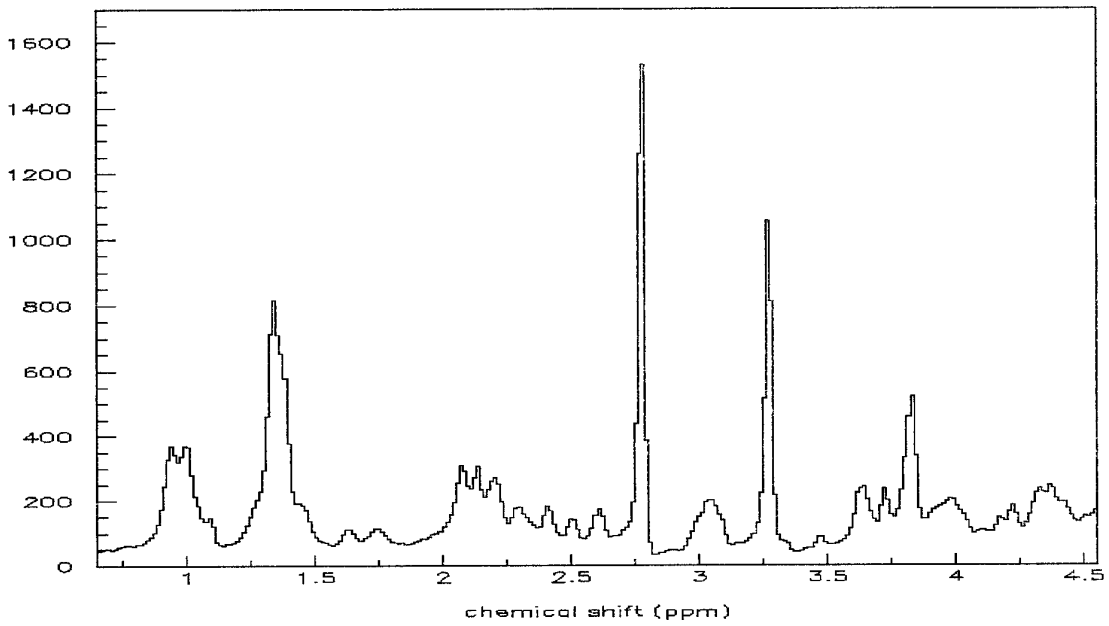

Figure 23. Diffusion-weighted (intra-cellular) ^{1}H MR spectrum of MCF7 breast cancer cells perfused at 37°. *Note that the spectrum is reversed in order to digitize the chemical shift scale.*

The three main regions of interest from the cell spectra that were chosen for detailed analysis are shown in **Figure 24**:

- The lactate region (1.1-1.5 ppm): fitted to 4 gaussian curves
- The creatine region (2.9-3.1 ppm): fitted to 2 gaussian curves
- The choline region (3.2-3.4 ppm): fitted to 2 gaussian curves

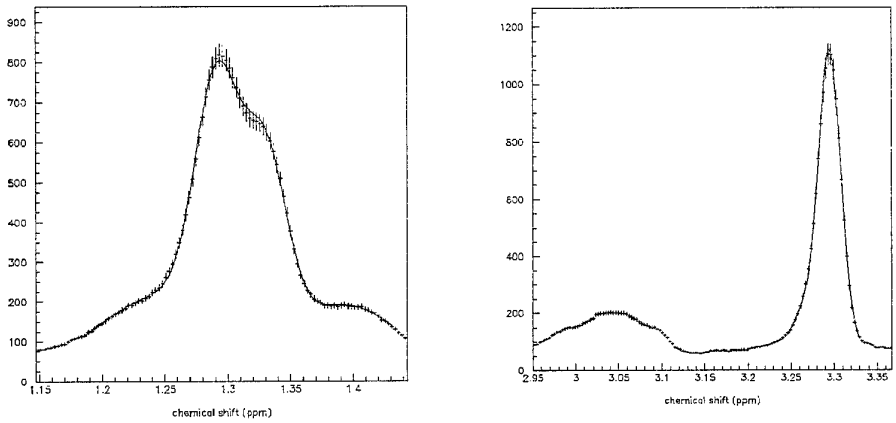

Figure 24. Regions of interest chosen from the spectrum shown in Fig. 23. Left: the lactate region. Middle: the creatine region. Right: the choline region.

Quantification of the peak intensities was obtained by fitting regions of interest in the spectra to functions consisting of gaussian curves (for the peaks) and polynomials (if necessary, for the baseline). **Figure 25** shows the details of the fit to the lactate region of MCF7 cells. The error bars in the spectrum were chosen to be 3% of the intensity. The chi-squared value was 0.4. The fit was performed to a function of four gaussian curves (the solid top line). The two wide low peaks (at 1.25 ppm and 1.4 ppm) are contributions from macromolecules. The narrow peak at 1.33 ppm is the lactate peak. The narrow peak at 1.29 ppm has not been assigned yet, but we believe it is either threonine or fucose (extracts could be done, but for these we cannot use DW spectroscopy, and the chemical shifts of the methylenes of these two compounds are essentially identical).

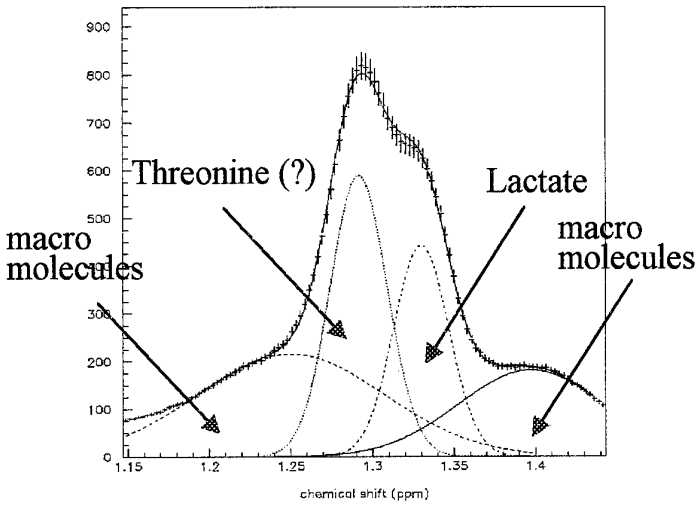

Figure 25. Fitting the lactate region of MCF7 cells. The spectrum was fitted to 4 gaussian shapes (at 1.25, 1.29, 1.33 and 1.4ppm). The widths (sigma) of the two central peaks are 0.0177 and 0.0174 ppm, consistent with metabolites. The widths of the two side peaks are 0.051 and 0.049 ppm, consistent with macromolecules.

In **Figure 26** (left histogram) we show the ratio between the choline region and the creatine region integrated signals, which are consistent for all cell lines. The qualitative difference between the cell groups in the ratio between the total lactate region and the choline region, shown in **Fig. 22**, is quantified in **Figure 26** (right histogram).

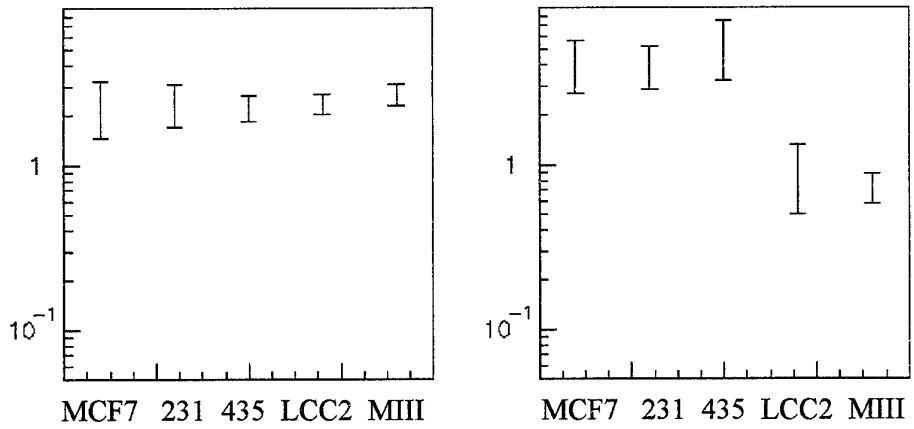

Figure 26. Quantitative comparison between DWMR spectra of five human breast cancer cell lines. The left histograms shows the ratio between the choline region and the creatine region. The right histogram shows the ratio between the lactate region and the choline region, for the first group of cell lines (MCF7, MB231 and MB435) and the second group (LCC2 and MIII).

In order to further investigate the origin of the difference between the cell lines shown in **Figure 26** (right), we used the areas of the fitted peaks it consists of – lactate, threonine/fucose and macro-molecules. We plotted the ratio between each one of these components and the choline region to see what is the contribution of each to the differences between the cell lines shown in **Fig. 26** (right). **Figure 27** shows that the contribution to the differences between cell lines from the threonine/fucose and the macro-molecule peaks is significant, while the lactate peak contributes less.

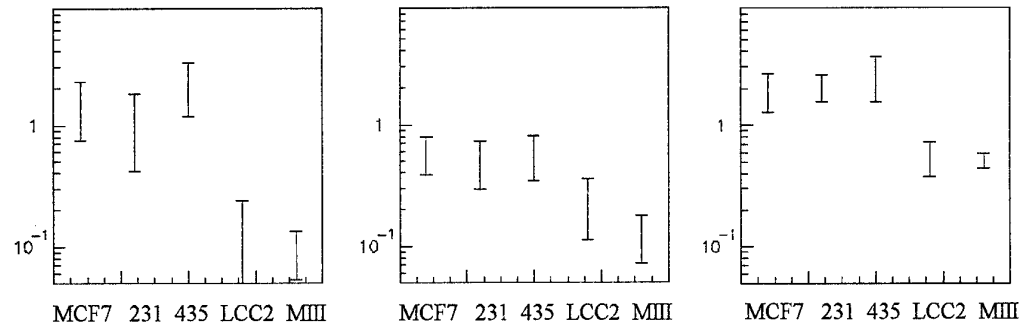

Figure 27. The contribution of the different peaks in the lactate region to the difference between the cell lines shown in Figure 26 (right). Left – the ratio between the threonine/fucose peak and the choline region. Middle – the ratio between the lactate peak and the choline region. Right – the ratio between the macro-molecule peaks and the choline region.

To conclude, we showed that with DWMRS we are able to separate the intra- from the extra-cellular MR signals, thus obtaining intra-cellular proton spectra of cells. We compared the spectra of 5 different human breast cancer cell lines and one mouse melanoma cell line. By means of curve fitting we found that while some peaks areas and ratios remain the same, we are able to show quantitative differences for certain peaks in the spectra of different groups of cell lines that differ in their hormonal properties. The biological significance of these differences cannot yet be understood.

(ix) Effects of Lonidamine on Lactate Levels in DWMR Spectra of Cells

The effect of the anti-neoplastic agent Lonidamine (LND) on the metabolism of perfused cancer cells was studied by DWMRS. Previous ^{31}P and ^{13}C MRS studies reported that this drug induced intra-cellular acidification and lactate accumulation (Ben-Horin et al., 1995; Vivi et al., 1997). The effects of LND on the intra-cellular lactate signal in three different cancer cell lines - MCF7 and MIII human breast cancer cells, and F10-9 murine melanoma cells - were studied. Diffusion-weighted spectra demonstrated a two to five fold higher intra-cellular lactate after LND treatment (**Figure 28**) compared to the control perfusions. No other proton spectral changes were observed following LND perfusion. A moderate decrease of the lactate signal in the perfusate was also observed in the water suppressed proton spectra of the effluent solution. Similar results were obtained with all three cancer cell lines. Therefore it may be concluded that the primary effect of LND in some cancer cells is marked inhibition of lactate transport, and this confirms the mechanism of action LND.

In order to test the effect of LND concentration on the metabolism of cancer cell lines, we perfused F10-9 murine melanoma cells with increasing concentrations of LND, waiting for the lactate level to reach a steady state before each measurement. LND does not dissolve well in water, therefore, we first dissolved it in DMSO (10 μl DMSO per mg LND) and then dissolved the LND-DMSO solution in PEG200 (100 μl per mg LND) before mixing it in the perfusion medium. The perfusion medium consisted of low glucose DMEM, 1 gm per liter, with the addition of 5% fetal calf serum. **Figure 29** shows the intensity of the lactate peak (arbitrary units) as a function of LND concentration (in mg per ml).

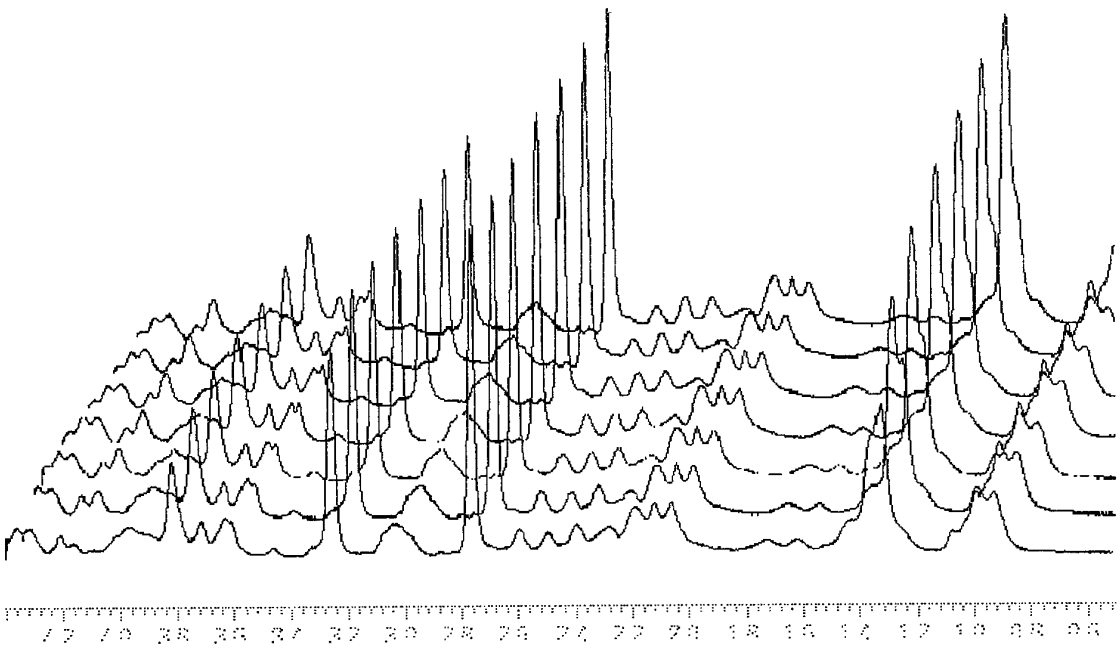

Figure 28. DWMR spectra of perfused MCF7 cells at 37°C. Each spectrum represents 20 minutes of accumulation. In the first spectrum cells were perfused with normal medium, then LND was added. Note the marked elevation of the lactate signal at 1.33 ppm following LND administration.

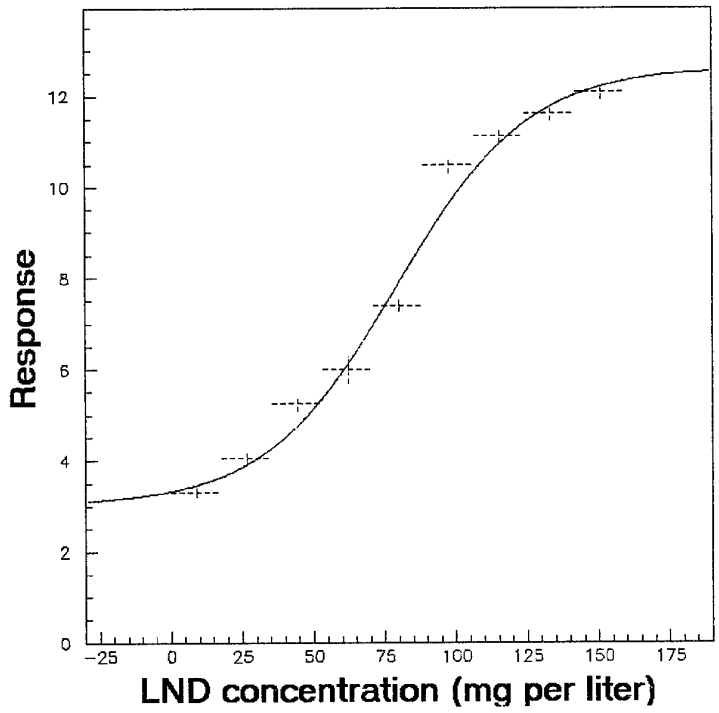

Figure 29. Concentration dependence of intra-cellular lactate on LND concentration. The lactate level (arbitrary units) as a function of the LND concentration (in mg per l medium). The cells were perfused at a flow rate of 1 ml per minute. The intra-cellular proton spectrum at each concentration point was measured after the system reached equilibrium. The lactate level at each point was obtained by fitting the lactate peak to a gaussian curve. The solid curve is a result of a fit to a sigmoid function (see text).

To determine the maximum value of LND response (by what factor did the lactate signal intensity increase) and the midpoint of the curve (the LND concentration value corresponding to 50% of the maximal response), we fitted the data to the following equation, derived from the Henderson-Hasselbach equation (Edsall and Wyman, 1958):

$$R = (R_{\max} + e^{a(C-Cmid)} R_{\min} / (1 + e^{a(C-Cmid)})$$

Where R is the lactate response, R_{max} and R_{min} are the maximal and minimal response values, C is the LND concentration and C_{mid} is the midpoint of the curve.

The results of the fit are shown in **Figure 29**, where

$$R_{\max} = 12.6 \pm 0.2$$
$$R_{\min} = 3.0 \pm 0.2$$
$$C_{mid} = 79.3 \pm 1.6$$

The maximal response to LND was an increase by 4.2 fold (12.6/3) of the lactate signal intensity and the midpoint of the response was an LND concentration of 80 mg/l. Therefore, we were able to obtain the dependence of the intra-cellular response to LND quantitatively.

C. Discussion

The intersection of a major health problem, namely breast cancer, and an advanced technology, namely MRS, deserves serious investigation. How and in what ways could MRS help us to understand and confront the challenges posed by breast cancer? The focus of much research in breast cancer today is on the genetics of the origin of the aberrant growth, and this involves studies of growth factors and their control. But, we also need to step back and observe the phenomenon with imaging and spectroscopy techniques that may give us insight into the more macroscopic origins of the disease. Such a method is MRS applied specifically to studies of cellular metabolism.

MRI is being applied to breast cancer (Hofmann et al., 1995), but MRI lacks the specificity needed to define the nature of a breast lesion. MRS could in principle provide that specificity, possibly in a single patient visit that includes an MR image, but so far MRS has failed to live up to its promise. There are several reasons for this, one is lack of sensitivity, another is lack of resolution of signals, and so on. This work was begun on the premise that we needed to carry out a detailed analysis of breast cancer cells by MRS, in an attempt to improve the understanding and possibly the clinical application to breast cancer, either to diagnosis or monitoring of therapy.

We chose the approach of embedding cells in various forms of gel, in order to be able to perfuse them and to observe the signals from the cellular aggregate. This represents in effect a "model tumor" where the cells are closely packed (although not quite at tissue density) and can be treated experimentally. The cell lines we chose were selected by Clarke et al. (1989) for their hormonal properties, paralleling intermediate stages in the progression of resistance of breast cancer to hormonal treatment. We also chose to extend our method to include the use of Matrigel (Kleinman et al, 1986), since cancer cells can proliferate in this matrix.

Our results divide into two main sections, first ^{31}P MRS studies and second ^{1}H MRS studies. The former is a well-developed technique that notwithstanding its limitations has been applied to many systems, including breast cancer cells (Ruiz-Cabello et al, 1994). The primary drawback of ^{31}P MRS is its lack of sensitivity, which means that any approach developed on a cellular system at high magnetic field strength (as here) would be hardly applicable at the lower strengths that are used and are achievable in whole body magnet systems for clinical use. Perhaps the smallest volume that could be observed by localized ^{31}P MRS would be ca. 16 cm^3. By contrast, ^{1}H MRS has greater intrinsic sensitivity, so that one could observe signals from a volume as small as 1 cm^3 (Roebuck et al., 1998). But, the large number of proton signals, and the consequent poor resolution, together with the huge water signal represent serious drawbacks to the development of this method. We have overcome these problems using the technique of diffusion weighting that enables us to observe only the signals from intra-cellular components.

Our results show that it is possible to obtain both high-resolution ^{31}P and ^{1}H spectra of cellular aggregates perfused in gels showing only the intra-cellular components in both cases. From the comparisons of various cell lines selected for hormonal differences, we were able to quantitative differences in the levels of specific metabolites, against a background of many metabolites that are not different. Among these the most notable were the UDPS and the phospho-diester (GPC and GPE) signals. Also, we were able to observe a significant increase in the levels of GPC upon treatment with Taxol and other drugs, and of lactate upon treatment with LND (see Results section for details). The role of non-cyclic phosphodiesters in cellular metabolism is poorly understood, but several functions have been proposed. These include: 1) phosphodiesters are degradation products of phospholipids; this is generally true, although GPC is low in muscle cells, and this correlates with a low level of phospholipase activity; 2) phosphodiesters may also be precursors in phospholipid biosynthesis; 3) phosphodiesters are endogenous inhibitors of phospholipase; 4) GPC may serve as a source of glycerol and/or choline; 5) GPC, which contains a methylamino group, is involved in osmoregulation (for reviews see Van den Thillart and Van Waarde, 1996; Ruiz-Cabello and Cohen, 1992). While further research is need to clarify these observations, we hope that they may shed some light on the mode of action of the drugs, and that these changes might have value as an indicator of clinical progress *in vivo*.

While we cannot predict the eventual outcome of the application of these studies, we do feel that the ability to recognize changes at the cellular level and to detect drug-related responses in near real-time represents an important step in the direction of the beneficial application of MRS (together with MRI) as a routine clinical modality in the diagnosis and treatment of breast cancer.

3. CONCLUSIONS

(a) We have found no significant effect of estrogen and tamoxifen on the growth curves of MIII cells and of estrogen on LCC2 cells grown in Matrigel.
(b) We compared baseline ^{31}P MR spectra of 5 breast cancer cell lines grown in Matrigel.
(c) We have noted a significant difference in the UDPS, GPC And GPE concentrations in MDA-MB231and MDA-MB435 cell lines, compared to LCC2, MIII and MCF7.
(d) Synchronization in G2/M by itself was not associated with significant changes in ^{31}P MR spectra.
(e) Elevation of intra-cellular GPC was observed for MDA-MB231 and MDA-MB435 cell lines (which have low basic levels of GPC and do not have ER) after treatment with anti-microtubule drugs (Taxol, Vincristine, Colchicine and Nocodazole). This elevation was not limited to the cells in Matrigel, but was also observed for cells embedded in alginate capsules and grown as monolayers.
(f) With an innovative combination of cell cycle synchronization and spectroscopy we showed that the elevation of GPC with drugs was not due to cell cycle effects or apoptosis, and was not due to membrane degradation.
(g) Diffusion weighted proton intra-cellular MR spectra have been obtained for 5 breast cancer cell lines.
(h) We were able to show quantitative differences for certain peaks in the spectra of different groups of cell lines that differ in their hormonal properties.
(i) Lonidamine gave an increase in intra-cellular lactate as observed directly by DWMRS, confirming the mechanism of action of this drug, and allowing determination of its concentration dependence.

4. REFERENCES

Ben-Horin H., Tassini, M., Vivi, A., Navon, G., and Kaplan, O. (1995) Mechanism of action of the antineoplastic drug lonidamine: ^{31}P and ^{13}C nuclear magnetic resonance studies. Cancer Res. 55:2814-2821,

Clarke, R., Brünner, N., Katzenellenbogen, B.S., Thompson, E.W., Norman, M.J., Koppi, C., Paik, S., Lippman, M.E., and Dickson, R. (1989) Progression of human breast cancer cells from hormone-dependent to hormone-independent growth both *in vitro* and *in vivo*. Proc. Natl. Acad. Sci. USA 86:3649-3653.

Clarke, R., Brünner, N., Thompson, E.W., Glanz, P., Katz, D., Dickson, R., and Lippman, M.E. (1989) The inter-relationships between ovarian-independent growth, tumorigenicity, invasiveness and anti-estrogen resistance in the malignant progression of human breast cancer. J. Endocrinol. 122: 331-340.

Clarke, R., Dickson, R., and Brünner, N. (1990) The process of malignant progression from hormone-dependence to interdependency in human breast cancer. Ann. Oncol. 1:401-407.

Cohen, J.S., Lyon, R.C., Chen, C., Faustino, P.J., Batist, G., Shoemaker, M., Rubalcaba, E., and Cowan, E.H. (1986) Differences in phosphate-metabolite levels in drug-sensitive and –resistant human breast cancer cell lines determined by ^{31}P magnetic resonance spectroscopy. Cancer Res. 46:4087-4090.

Cohen, J.S., Lyon, R.C., and Daly, P.F. (1989) Monitoring intra-cellular metabolism by NMR. Methods Enzymol. 177:435-438.

Cohen, J.S., Jaroszewski, J., Kaplan, O., Ruiz-Cabello, J., and Collier, S. (1995) A History of Biological Magnetic Resonance. Progr. Magn. Reson. (50th ann. edition of discovery of NMR) (Emsley and Feeney, eds.) 28: 53-86.

Cushman, M., He, H.M., Katzenellenbogen, J.A., Lin, C.M., and Hamel, E. (1995) Synthesis, anti-tubulin and anti-mitotic activity, and cytotoxicity of analogs of 2-methoxyestradiol, an endogenous mammalian metabolite of estradiol that inhibits tubulin polymerization by binding to the colchicine binding site. J. Med. Chem., 38:2041-2049.

Daly, P., and Cohen, J.S. (1989) Magnetic resonance spectroscopy of tumors and potential in vivo clinical applications: a review. Cancer Res. 49:770-779.

Daly, P., Lyon, R.C., Straka, E.J., and Cohen, J.S. (1988) ^{31}P NMR spectroscopy of human cancer cells proliferating in a basement membrane gel. FASEB J. 2:2596-2604.

Edsall J.T. and Wyman J. (1958) Biophysical Chemistry, Vol. 1, Chap. 8.

Evelhoch, J.L., Keller, N.A., and Corbett, T.H. (1987) Response-specific adriamycin sensitivity markers provided by in vivo 31P nuclear magnetic resonance spectroscopy in murine mammary adenocarcinomas. Cancer Res. 47:3396-3401.

Foxall, D.L., Cohen, J.S., and Mitchell, J.B. (1984) Continuous perfusion of mammalian Cells embedded in agarose gel threads. Exp. Cell Res. 154:521-529.

Foxall, D.L., and Cohen, J.S. (1983) NMR studies of perfused cells. J. Mag. Res. 52:346-349.

Gosland, M, Tsuboi, C., Hoffman, T., Goodin, S., and Vore, M. (1993) 17 beta-estradiol glucuronide: an inducer of cholestasis and a physiological substrate for the multidrug resistance transporter. Cancer Res., 53: 5382-5385.

Hardy, S.P., and Valverde, M.A. (1994) Novel plasma membrane action of estrogen and antiestrogens revealed by their regulation of a large conductance chloride channel. FASEB J., 8: 760-765.

Hofmann, U., Brix, G., Knopp, M.V., Hess, T., and Lorenz, W.J. (1985) Pharmacokinetic mapping of the breast: a new method for dynamic MR mammography Mar. Reson. Med. 33:506-514.

Kaplan, O., and Cohen, J.S. (1991) Lymphocyte activation and phospholipid pathways; 31P MRS studies. J. Biol. Chem. 266:3228-3232.

Kaplan, O., van Zijl, P.C.M., and Cohen, J.S. (1990) Information from combined ^{1}H and ^{31}P NMR studies of cell extracts: differences between drug-sensitive and drug-resistant MCF-7 human breast cancer cells. Biochem. Biophys. Res. Comm. 169:383-390.

Kibbey, M.C. (1994) Maintenance of EHS sarcoma and Matrigel preparation. J. Tissue Culture Methods 16:227-230.

Kirk, J., Houlbrook, S., Stuart, N.S., Stratford, I.J., Harris, A.L., Carmichael, J. (1993) Selective reversal of vinblastine resistance in multidrug-resistant cell lines by tamoxifen, toremifene and their metabolites. Eur. J. Cancer 29A: 1152-1157.

Kleinman, H.K., McGarvey, M.L., Hassell, J.R., Star, V.L., Cannon, F.B., and Laurie, G.W. (1986) Basement membranes with biological activity. Biochemistry 25:312-318.

Knop, R., Chen, C.-W, Mitchell, J.B., Russo, A., McPherson, S., and Cohen, J.S. (1984) Metabolic studies of mammalian cells by ^{31}P NMR using a continous perfusion technique. Biochim. Biophys. Acta 894:275-284.

Koester, S.K., Maenpaa, J.U. Wiebe, V.J., Baker, W.J., Wurz, G.T., Seymour,R.C., Koehler, R.E., and DeGregorio, M.W. (1994) Flow cytometry: potential utility in monitoring drug effects in breast cancer. Breast Cancer Res Treat. 32: 57-65.

Kvistad, K.A., Bakken, I.J., Gribbestad, M.S., Ernholm, B., Lundgren, S., Fjosne, H.E., and Haraldseth, O. (1999) J. Mag. Res. Imaging 10:159-164.

Leonessa, F., Jacobson, M., Boyle, B., Lippman, J., McGarvey, M., and Clarke, R. (1994) Effect of tamoxifen on the multidrug-resistant phenotype in human breast cancer cells: isobologram, drug accumulation, and M(r) 170,000 glycoprotein (gp170) binding studies. Cancer Res., 54: 441-447.

Levenson, A.S., and Jordan, V.C. (1997) MCF-7: the first hormone-responsive breast cancer cell line. Cancer Res. 57:3071-3078.

Lim, F., and Moss, R.D. (1981) Microencapsulation of living cells and tissues. J. Pharm. Sci. 70:351-354.

Lyon, R.C., Faustino, P.J., and Cohen, J.S. (1986) A perfusion technique for ^{13}C NMR studies of the metabolism of ^{13}C-labeled substrates by mammalian cells. Mag. Reson. Med. 3:663-672.

Meneses, P., and Glonek, T. (1988) High resolution ^{31}P NMR of extracted phospholipids. J. Lipid Res. 29:679-689.

McGuire, W.P. and Rowinsky, E.K.; eds (1995) Taxol in Cancer Treatment, Marcel Dekker Inc. New York.

Moonen, C.T., and Van Zijl, P.C.M. (1990) Highly effective water suppression for in vivo proton MR spectroscopy. 88:28-41.

Moran, P. R. (1982) A flow velocity zeugmatographic interlace for NMR imaging in humans. Mag. Res. Imaging 1:197-203.

Parikh, I., Rajendran, K.B., Su, J.L., Lopez, T., and Sar, M. (1987) Are estrogen receptors cytoplasmic or nuclear? Some immunocytochemical and biochemical studies. J. Steroid Biochem. 27: 185-192.

Roebuck, J.R., Cecil, K.M., Schnall, M.D., and Lenkinski, R.E. (1998) Human breast lesions: characterization with proton MR spectroscopy. Radiology 209:269-275.

Ruiz-Cabello, J., Berghmans, K., Kaplan, O., Lippman, M., Clarke, R., and Cohen, J.S. (1994) Hormone Dependence of breast cancer cells and the effects of tamoxifen and estrogen: ^{31}P NMR studies. Breast Cancer Res. & Treat.33:209-217.

Ruiz-Cabello, J., and Cohen, J.S. (1992) Phospholipid metabolites as indicators of cancer cell function. NMR in Biomedicine 5:226-233.

Shankar-Narayan, K., Moress, E.A., Chatam, J.C., and Barker, P.B. (1990) ^{31}P NMR of mammalian cells encapsulated in alginate gels utilizing a new phosphate-free perfusion medium. NMR Biomed. 3:23-26.

Stejskal, E. O. and Tanner, J. E. (1965) Spin diffusion: spin echoes iun the presence of a time-dependent field gradient. J. Chem. Phys. 42:288-292.

Tyagi, R.K., Azrad, A., Degani, H., and Salomon, Y. (1996) Simultaneous extraction of cellular lipids and water-soluble metabolites: evaluation by NMR spectroscopy. Mag. Reson. Med. 35:196-200.

Van Den Thillart, G., and Van Waarde, A. (1996) Nuclear magnetic resonance spectroscopy of living systems: applications in comparative physiology. Physiol. Rev. 76:799-837.

Van Zijl, P.C., Moonen, C.T., Faustino, P., Pekar, J., Kaplan, O., and Cohen, J.S. (1991) Complete separation of intra-cellular and extra-cellular information in NMR spectra of perfused cells by diffusion-weighted spectroscopy. Proc. Natl. Acad. Sci. 88:3228-3232.

Vivi, A. Tassini, M., Ben-Horin, H., Navon, G., and Kaplan, O. (1997) Comparison of action of the anti-neoplastic drug lonidamine on drug-sensitive and drug-resistant human breast cancer cells: ^{31}P and ^{13}C nuclear magnetic resonance studies. Breast Cancer Res. & Treat. 43:15-25.

Wilson, L. and Jordan, M.A. (1994) Pharmacological probes of microtubule function in: Microtubules (Hymas and Lloyd, eds.) pp. 59-83.

Wong, K. and Henderson, I.C. (1994) Management of metastatic breast cancer. World J Surg.18:98-111.

5. Abbreviations Used:

Note that names of cells lines are not abbreviations.
^{31}P, phosphorus-31; ADP, adenosine diphosphate; ATP, adenosine triphosphate; CHESS, chemical shift selective; DW, diffusion weighted; ER, estrogen receptor; GPC, glycerylphosphocholine; GPE, glycerylphosphoethanolamine; LND, lonidamine; MHz, megaHertz; MRI, magnetic resonance imaging; MRS, magnetic resonance spectroscopy; NADP, nicotine adenine diphosphate; NMR, nuclear magnetic resonance; PBS, phosphate buffered saline; PCr, phosphocreatine; PC, phosphorylcholine; PD, phosphodiesters; Pi, inorganic phosphate; PM, phosphomonoesters; PtdC. Phosphatidylcholine; PtdE, phosphatidylethanolamine; PtdI, phosphatidylinositol; PtDS. phosphatidylserine; Plasm, plasmalogens; rf. radiofrequency; SPM, sphingomyelin; UDPG, uridine diphosphoglucose; UDPS, uridine diphospho-sugar.

6. Publications and Personnel

1. Sterin, M., Cohen, J.S., Mardor, Y., Berman, E., and Ringel, I. Levels of phospholipid metabolites in breast cancer cells treated with anti-mitotic drugs: a ^{31}P magnetic resonance spectroscopy study. Abstract at Hormones & Cancer Meeting, Jerusalem, September, 1999.
2. Mardor, Y., Kaplan, O., Sterin, M., Ruiz-Cabello, J., Ash, E., Ringel, I., and Cohen J.S.. Diffusion weighted proton MRS: applications to cell metabolism and oncologic pharmacology. Abstract at Hormones & Cancer Meeting, Jerusalem, September, 1999.
   Note: This Poster won the First Prize for Excellence in the Breast Cancer Category
3. Sterin, M., Cohen, J.S., Mardor, Y., Berman, E., and Ringel, I. Levels of phospholipid metabolites in breast cancer cells treated with anti-mitotic drugs: a ^{31}P magnetic resonance spectroscopy study, ms in preparation.
4. Mardor, Y., Kaplan, O., Sterin, M., Ruiz-Cabello, J., Ash, E., Ringel, I., and Cohen J.S.. Diffusion weighted proton MRS: applications to cell metabolism and oncologic pharmacology, ms in preparation.

The following personnel have been engaged in this project:

Jack S. Cohen	PI	GU and Sheba Med Center	1994-99
Israel Ringel	CI	Hadassah Med Center-HU	1995-99
Marina Sterin	Grad Student	Hadassah Med Center-HU	1995-99
Yael Mardor	Post-doc	Sheba Med Center	1997-99
Ofer Kaplan	CI	Ichilov Hospital, Tel Aviv	1999
Jesus Ruiz-Cabello	CI	Madrid, Spain	1997-99
Sharona Salomon	Tech	Sheba Med Center	1998-99
Elissa Ash	Grad student	Tufts Univ. Boston	1998